J. Fluid Mech. (2002), *vol.* 466, *pp.* 215–248.
DOI: 10.1017/S0022112002001271 Printed in the United Kingdom

Experiments on Lagrangian transport in steady vortex-breakdown bubbles in a confined swirling flow

By FOTIS SOTIROPOULOS, DONALD R. WEBSTER AND TAHIRIH C. LACKEY

School of Civil and Environmental Engineering, Environmental Fluid Mechanics and Water Resources, Georgia Institute of Technology, Atlanta, GA 30332–0355, USA

(Received 20 March 2001 and in revised form 20 March 2002)

In a recent study, Sotiropoulos *et al.* (2001) studied numerically the chaotic particle paths in the interior of stationary vortex-breakdown bubbles that form in a closed cylindrical container with a rotating lid. Here we report the first experimental verification of these numerical findings along with new insights into the dynamics of vortex-breakdown bubbles. We visualize the Lagrangian transport within the bubbles using planar laser-induced fluorescence (LIF) and show that even though the flow fields are steady – from the Eulerian standpoint – the spatial distribution of the dye tracer varies continuously, and in a seemingly random manner, over very long observation intervals. This finding is consistent with the arbitrarily long Šil'nikov transients of upstream-originating orbits documented numerically by Sotiropoulos *et al.* (2001). Sequences of instantaneous LIF images also show that the steady bubbles exchange fluid with the outer flow via random bursting events during which blobs of dye exit the bubble through the spiral-in saddle. We construct experimental Poincaré maps by time-averaging a sufficiently long sequence of instantaneous LIF images. Ergodic theory concepts (Mezić & Sotiropoulos 2002) can be used to formally show that the level sets of the resulting time-averaged light intensity field reveal the invariant sets (unmixed islands) of the flow. The experimental Poincaré maps are in good agreement with the numerical computations. We apply this method to visualize the dynamics in the interior of the vortex-breakdown bubble that forms in the wake of the first bubble for governing parameters in the steady, two-bubble regime. In striking contrast with the asymmetric image obtained for the first bubble, the time-averaged light intensity field for the second bubble is remarkably axisymmetric. Numerical computations confirm this finding and further reveal that the apparent axisymmetry of this bubble is due to the fact that orbits in its interior exhibit quasi-periodic dynamics. We argue that this stark contrast in dynamics should be attributed to differences in the swirl-to-axial velocity ratio in the vicinity of each bubble. By studying the bifurcations of a simple dynamical system, with manifold topology resembling that of a vortex-breakdown bubble, we show that sufficiently high swirl intensities can stabilize the chaotic orbits, leading to quasi-periodic dynamics.

1. Introduction

Vortex breakdown has been among the most widely studied fluid mechanics phenomena since it was first discovered to occur over delta wings by Peckham & Atkinson (1957). The term is typically used to denote a very complex and abrupt transformation

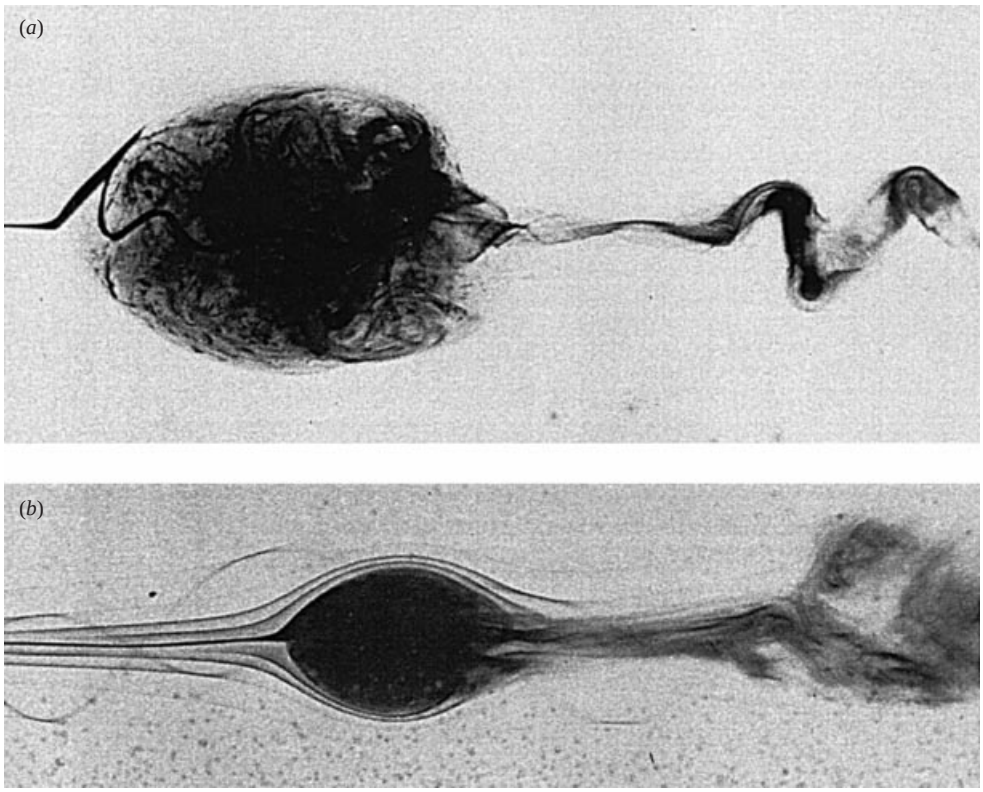

FIGURE 1. Visualization of vortex-breakdown bubbles in swirling flow through a circular diffuser. (*a*) $Re = 3400$, swirl ratio = 1.75; (*b*) $Re = 3800$, swirl ratio = 1.75 (Sarpkaya 1971*a* and private communication).

of a columnar vortex into a much larger structure, which could involve recirculation and unsteadiness. The numerous areas of engineering practice where vortex breakdown is important, along with its multifaceted aspects that still elude a comprehensive theory, are well known and documented in a series of review papers by Leibovich (1978, 1984), Escudier (1988), Delery (1994), and Sarpkaya (1995).

The various modes of vortex breakdown were identified in the pioneering flow visualization experiments by Sarpkaya (1971*a*, *b*) and Faler & Leibovich (1977) and essentially include the double helix, bubble, and spiral forms – see Faler & Leibovich (1977) for a more detailed classification. Perhaps the most intriguing and still poorly understood of these modes is the 'axisymmetric' bubble-like disturbance, known as the vortex-breakdown bubble. Figure 1 shows two of Sarpkaya's (1971*a*) dye-visualization photographs of such bubbles in a straight circular diffuser. Sarpkaya (1971*a*, *b*), among others, pointed out that: (i) the flow in the interior of the bubbles is unsteady and is dominated by the gyrations of a tilted toroidal ring; (ii) the bubbles exchange fluid with the ambient flow via unsteady fluctuations through their open downstream end; and (iii) certain combinations of swirl intensity and Reynolds number yield smoother and more axisymmetric bubble shapes (figures 1*a* and 1*b*). Faler & Leibovich (1977) subsequently verified many of Sarpkaya's observations and described in more detail the highly unsteady motion of a corkscrew-like dye filament along the axis in the interior of the bubble. Faler & Leibovich (1977) reported that this spiral filament appeared and disappeared in a random fashion in their experiment.

It is important to recognize that a great deal of what we know today about vortex breakdown has been derived from laboratory dye visualization experiments such as the one shown in figure 1. That is, conclusions concerning fundamental Eulerian aspects of the phenomenon (steady or inherently unsteady, axisymmetric vs. three-dimensional, etc.) have been largely based on Lagrangian visualizations of the flow fields. It is known, however, that Lagrangian and Eulerian descriptions of the same flow field can lead to drastically different conclusions about its complexity. Aref (1984) coined the term chaotic advection to describe such situations, where an innocuous, from the Eulerian standpoint, velocity field – such as a time-periodic two- or three-dimensional flow or even a steady three-dimensional flow – gives rise to chaotic Lagrangian dynamics. The first evidence that vortex-breakdown bubbles exhibit chaotic particle paths was reported in the recent study by Sotiropoulos, Ventikos & Lackey (2001) who studied numerically the Lagrangian characteristics of steady breakdown bubbles in a closed cylindrical container with a rotating lid – see Escudier (1984) for benchmark experiments and Spohn, Mory & Hopfinger (1998) and Sotiropoulos & Ventikos (2001) for a detailed discussion of this flow. Sotiropoulos *et al.* (2001) showed that the dynamics in the interior of stationary vortex-breakdown bubbles is consistent with what one would anticipate for a mildly perturbed, volume-preserving dynamical system: KAM-tori, cantori, and periodic islands were found embedded within chaotic regions. They argued that the onset of chaos in such flows is a manifestation of Šil'nikov's (1965) phenomenon and provided evidence pointing to the conclusion that a subset of measure zero of the total flux into the bubble may stay in its interior arbitrarily long.

Some experimental evidence supporting the findings of Sotiropoulos *et al.* (2001) was reported by Spohn *et al.* (1998) who showed that vortex-breakdown bubbles in the container flow are open and asymmetric at their downstream end. Although Spohn *et al.* (1998) did not link their findings to chaotic Lagrangian transport, the good agreement between their visualization photographs and the computed streaklines reported in Sotiropoulos & Ventikos (2001), along with the detailed analysis of the topology of the flow by Sotiropoulos *et al.* (2001), clearly establishes such a link. It should be emphasized, however, that direct laboratory evidence confirming the numerically identified rich Lagrangian dynamics in the interior of the bubbles has yet to be reported.

The objective of this work is to provide the first experimental evidence establishing the chaotic nature of the flow in the interior of vortex-breakdown bubbles. We carry out flow visualization experiments for two container aspect ratios and for various Reynolds numbers using the laser-induced fluorescence (LIF) technique. We collect and analyse long time-series of instantaneous LIF images and show that the dye tracer motion in the interior of steady vortex-breakdown bubbles exhibits very long transients. We also show that dye tracer does not exit the bubble through the spiral-in saddle in a continuous manner but rather in a sequence of random bursting events. We construct experimental Poincaré maps by time-averaging a sufficiently long time-series of such images and plotting the level sets of the resulting time-averaged light intensity field (Mezić & Sotiropoulos 2002). Applying this technique to study the dynamics within vortex-breakdown bubbles in the steady, two-bubble regime, we show that in striking contrast with the chaotic dynamics of the first bubble, orbits within the second bubble remain confined on invariant quasi-periodic tori. We offer an explanation for this surprising result by showing that sufficiently high swirl intensity can re-organize the chaotic orbits and lead to quasi-periodic dynamics. We also discuss observations from previous vortex-breakdown experiments in diffuser geometries in the light of the new findings reported herein.

The paper is organized as follows. In § 2 we discuss the phenomenon of vortex breakdown from a dynamical systems point of view. In § 3 we describe our laboratory apparatus and discuss the details of the various experimental procedures. In § 4 we outline the experimental methodology for constructing Poincaré maps. In § 5 we describe briefly the numerical method for obtaining the velocity fields and calculating the particle paths. In § 6 we present and discuss the results of our experiments along with some new computational findings that reinforce and clarify the laboratory observations. In § 7 we show that many of our laboratory and computational findings can be explained by studying the bifurcations of a simple dynamical system whose manifold structure resembles that of a vortex-breakdown bubble. Closing remarks and a discussion of our findings in the context of previous laboratory experiments in diffuser geometries are given in § 8.

2. Vortex breakdown: a dynamical systems point of view

In this section, we present a brief review of previous work in the area of dynamical systems that is directly relevant to the findings we report herein (see Sotiropoulos *et al.* 2001 for more details). The issues and concepts discussed in this section provide the theoretical framework for interpreting our computational and experimental findings.

The topology of a steady axisymmetric vortex-breakdown bubble consists of two fixed hyperbolic points (stagnation points) and their respective stable and unstable manifolds (Holmes 1984). The bubble surface is invariant (not accessible by upstream-originating orbits) and its interior is foliated by invariant KAM-tori (the stream-surfaces of the axisymmetric flow). That is, orbits in the interior of the bubble remain confined on their respective tori and chaotic advection is not possible. If such a flow structure could be realized in a laboratory experiment, upstream-originating dye tracer would not be able to penetrate the bubble surface – at least not within an interval shorter than molecular diffusion time scales. In any laboratory experiment, however, small non-axisymmetric disturbances are bound to be present even when great care is taken to design the apparatus and conduct the experiment (see extensive discussion in Stevens *et al.* 1996). It is known from the theory of dynamical systems (see for example Broer & Vetger 1984; Mezić & Wiggins 1994) that such disturbances, even when their magnitude is arbitrarily small, could drastically alter the Lagrangian properties of the flow by destroying the invariant stream-surfaces and leading to very rich, chaotic dynamics.

Holmes (1984) was the first to suggest that the dynamics of an axisymmetric vortex-breakdown bubble could be drastically altered by considering the effect of arbitrarily small time-periodic perturbations. Such disturbances would destroy the invariance of the bubble-like surface with orbits entering the bubble through its downstream end and recirculating in its interior for arbitrarily long times before they finally exit. Holmes considered in his analysis only the effects of time-periodic perturbations but as shown by Broer & Vetger (1984) even stationary disturbances could give rise to a very complex spatially chaotic flow via the mechanism discovered by Šil'nikov (1965) – see Sotiropoulos *et al.* (2001) for a detailed discussion of the Šil'nikov mechanism in the context of vortex breakdown. In a more recent study, MacKay (1994) further argued that a subset of measure zero (i.e. a Cantor set) of the total flux into a perturbed stationary bubble could remain trapped in its interior for arbitrarily long times. These theoretical developments have important implications for laboratory visualizations of vortex breakdown structures. For instance, such experiments using dye-based techniques could reveal complexities that can neither be explained nor

quantified by simply examining the properties of the Eulerian velocity field. Since even an arbitrarily small steady non-axisymmetric perturbation of a steady axisymmetric vortex-breakdown bubble could give rise to chaotic dynamics, one may observe in the laboratory very complex spatial and temporal variations of the dye tracer even though the transporting flow is stationary and 'nearly' axisymmetric. MacKay's (1994) conjectures further suggest that Lagrangian transients in the laboratory may persist for arbitrarily long times – of course, a cut-off time in a real experiment will be set by molecular diffusion – thus, creating an impression of 'unsteady' flow.

Perhaps the best example of this seemingly paradoxical behaviour is the flow in a closed cylindrical container with a rotating lid, for which the first comprehensive flow visualization experiments were reported by Escudier (1984) – see Goldshtik, Husain & Hussain (1992), Husain, Hussain & Goldshtik (1995), Spohn *et al.* (1993, 1998), and Stevens, Lopez & Cantwell (1999) for more recent experimental studies of various aspects of this flow. Escudier's experiments revealed that for container aspect ratios $H/R > 1.5$ (where H is the cylinder length and R is the cylinder radius) there is a threshold Reynolds number ($Re = \Omega R^2/\nu$ where Ω is the lid angular velocity and ν is the kinematic viscosity of the fluid) above which one or more stationary vortex-breakdown bubbles form along the container axis. Escudier's photographs show that a considerable quantity of fluorescent dye has penetrated the interior of the bubble, thus suggesting that the bubble-like surface of the laboratory structure is not invariant. Furthermore, there are distinct asymmetric folds at the downstream end of the bubble, which are remarkably similar to those shown in the sketch of Broer & Vetger (1984) – see figure 8 in Sotiropoulos *et al.* 2001. Yet numerical solutions of the axisymmetric Navier–Stokes equations capture with good accuracy the general flow patterns and the evolution of these patterns with Reynolds number and container aspect ratio, observed in the laboratory both in the steady and unsteady flow regimes (e.g. Lopez 1990; Lopez & Perry 1992; Gelfgat *et al.* 1996; Stevens *et al.* 1999). Axisymmetric streamlines, of course, cannot reproduce the asymmetric dye-tracer patterns observed in the laboratory. Recent experiments (Spohn *et al.* 1998) and three-dimensional numerical simulations (Sotiropoulos & Ventikos 2001; Sotiropoulos *et al.* 2001) explained the origin of these asymmetries and showed that the flow in the interior of steady vortex-breakdown bubbles exhibits chaotic particle paths and very rich Lagrangian dynamics. In the subsequent sections of this paper, we will provide experimental and additional computational evidence that further clarify the issues discussed herein.

3. Experimental apparatus and flow visualization method

Experiments have been performed in a carefully constructed tank facility, shown in figure 2. The test cell consisted of a cast acrylic cylinder with inner diameter of 203.2 ± 0.05 mm. The cylinder was submerged in a rectangular tank containing the test fluid, thus minimizing optical distortions. In this case the index of refraction of the fluid did not match the acrylic cylinder, thus slight distortions of the visualization occurred due to light passing through the cylinder wall. The height of the non-rotating Plexiglas endwall was adjustable between $H/R = 1$ and 4.

A variable-speed DC motor rotated the lower endwall of the test cell at speeds up to 146 r.p.m. The surface of the rotating endwall was machined smooth; variation in the surface height varied less than ± 0.02 mm during rotation. The gap between the rotating endwall and the cylinder wall was 0.35 ± 0.05 mm. The motor speed was set by a TTL control voltage signal provided to the DC motor controller.

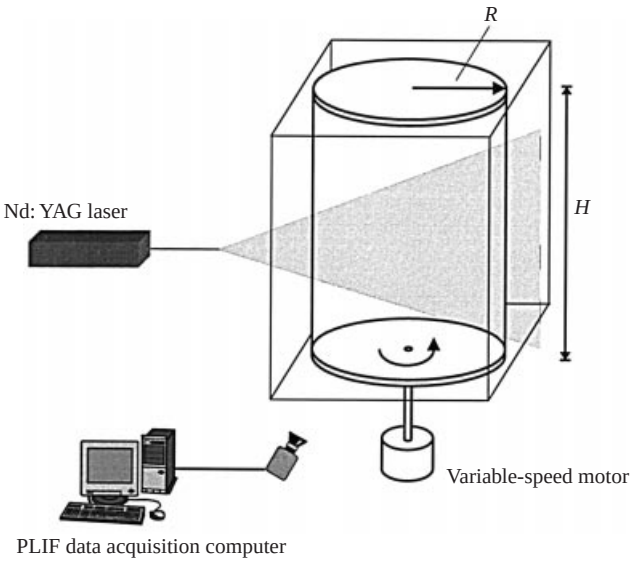

FIGURE 2. A schematic of the experimental apparatus.

The working solution was a glycerin/water mixture (roughly 3/1 by volume). The viscosity of the mixture was in the neighbourhood of 50 cP at 25 °C and was measured using a precision falling-ball viscometer at several temperatures over a range of 10 °C. The fluid temperature was measured during the experiment to within 0.1 °C in order to determine the viscosity. A precision mercury thermometer, submerged in the rectangular tank immediately adjacent to the test volume, was used to measure the temperature. Under normal experimental conditions, the fluid temperature in the apparatus was maintained to within 0.1 °C for several hours.

Flow visualization was performed using the planar laser-induced fluorescence (PLIF) technique. The dye solution consisted of the glycerin/water mixture with Rhodamine 6G at a concentration of $500\,\mu g\,l^{-1}$. The dye concentration was sufficiently low to minimize absorption effects. Dye was delivered to the flow through a 1.0 mm hole at the centre of the non-rotating endwall from a dye reservoir elevated 1.5 m above the experiment. The dye flow rate was extremely small, essentially matching the local flow velocity, in order to minimize perturbations to the container flow. Note that if the dye flow rate exceeded this iso-kinetic release, the resulting jet of dye adversely perturbed the bubble and the effects of the perturbation were obvious by visual inspection. For instance, excessive dye flow rates would not only change the location and overall shape of the bubble but also lead to the onset of visible unsteadiness (with the bubble darting up and down along the axis) even for governing parameters in the steady flow regime.

An illumination sheet was generated with a pulsed Nd:YAG laser. The pulse energy was 50 mJ and the sheet was formed by a combination of spherical and cylindrical lenses such that the laser sheet was approximately 1 mm thick in the imaged region. The laser sheet was vertically centred on each bubble before collecting data in order to provide as uniform a distribution of incident light intensity as possible. This was a critical step because the Lagrangian transport is quantified in terms of the intensity of emitted light, which is proportional to both the dye concentration and incident laser light intensity.

A Kodak digital camera acquired the emitted light. A Tiffen Orange 21 filter was used to block the green laser light, while passing the emitted yellow-orange light. The 1024×1024 pixel camera was tethered to a high-speed image capture board inside a Pentium-based computer. Images were streamed directly to the hard drive array, thus the computer RAM did not limit the number of images that could be collected. Unless otherwise noted, the image capture rate for these data was 2.0 frames per second, totalling 1440 images for each case. The image resolution ranged between 6.1 and 14.3 pixels mm^{-1} as dictated by the size of the individual bubbles.

We exercised great care to ensure that the dye injection hole was placed as close to the centre of the stationary cover as possible. It has been previously argued in the literature that the asymmetric aspects of vortex breakdown in the container geometry may be artifacts of the visualization technique due to the inability to locate the dye release hole exactly on the container centreline (Hourigan, Graham & Thompson 1995; Stevens *et al.* 1999). As we have already discussed in detail in Sotiropoulos & Ventikos (2001) and Sotiropoulos *et al.* (2001) and will further show in the subsequent sections of this paper, all our experimental findings are supported by the results of three-dimensional computations in which Lagrangian markers can be introduced precisely on the centreline or distributed in a perfectly axisymmetric manner around it. Moreover, and as has already been demonstrated experimentally by Spohn *et al.* (1998), the fact that the downstream end of the bubble is open and asymmetric is a structural feature of vortex breakdown and not an artifact of a particular visualization. Therefore, while uncertainties due to the placement of the dye-injection release hole cannot be entirely eliminated, they do not influence any of the findings we report in the subsequent sections of this paper.

We also attempted to eliminate, or at least minimize as much as possible, asymmetries of the experimental apparatus that could affect the visualized flow structures. It is important to note that the shape of the characteristic asymmetric folds at the downstream end of the bubble is extremely sensitive to very small experimental imperfections. Figure 3 depicts the results of two experimental runs for $Re = 1850$ and $H/R = 1.75$. The vortex-breakdown bubble shown in figure 3(a) was obtained after carefully minimizing all apparatus imperfections. The bubble shape shown in figure 3(b), on the other hand, emerged when a controlled asymmetric forcing was introduced into the flow field by slightly tilting the stationary cover by approximately 0.4°. Following the introduction of this perturbation and after the initial transients decayed, the steady-state flow structure shown in figure 3(b) emerged. Note that although the location and overall size of the two bubbles are very similar, the asymmetric forcing has a profound effect on the structure of the downstream asymmetric folds. Compared to the unperturbed case (figure 3a), the spiral-in saddle of the perturbed vortex-breakdown bubble appears to be more 'open' and is characterized by more intense and clearly visible asymmetric folds. Moreover, the wake of the perturbed bubble appears wider and the spiralling of the dye sheet is far more pronounced. The apparent extreme sensitivity of the manifold structure of the spiral-in saddle to small asymmetric forcing should not be surprising in the light of the critical role of the Šil'nikov mechanism in breaking the invariance of the bubble surface (Sotiropoulos *et al.* 2001) – see further discussion in § 7 below. All subsequently presented experiments have been carried out without any explicit asymmetric forcing, other than, of course, the small imperfections that are bound to remain in our apparatus even when great care is taken to eliminate them (see Stevens *et al.* 1996 for a detailed discussion of various sources of such asymmetries).

To validate our apparatus and ensure that the various uncertainties discussed above

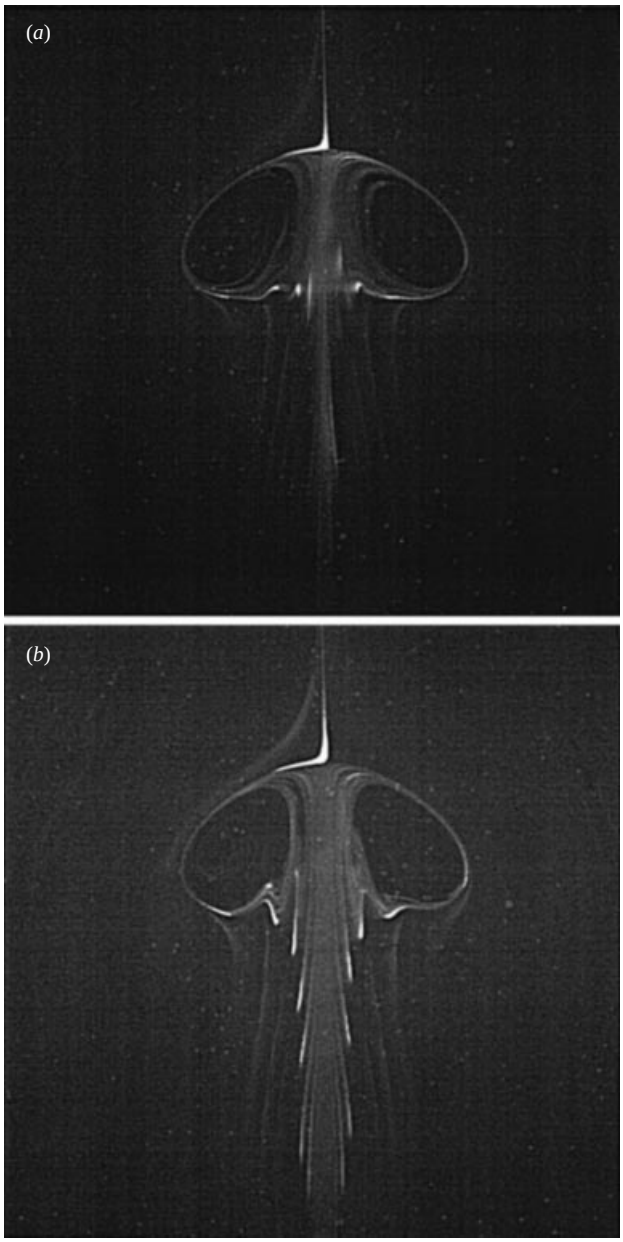

FIGURE 3. Visualized steady vortex-breakdown bubbles ($Re = 1850$, $H/R = 1.75$) in (a) a 'perfect' container; and (b) a container with the stationary lid tilted by approximately 0.4° from horizontal. Bubble diameter is $0.49R$.

(e.g. dye injection flow rate, temperature variations, apparatus asymmetries, etc.) do not adversely impact the accuracy of our results, we ran a series of experiments for two container aspect ratios ($H/R = 1.75$ and 2.0) over a broad range of Reynolds numbers. We found that both the variation of flow structures with Re and H/R and the number, overall size, shape and location of the vortex-breakdown bubbles are in excellent agreement with Escudier's (1984) benchmark experiments for this flow.

To further validate our apparatus, the LIF images demonstrated excellent agreement with superimposed calculated flow streamlines for all *Re*.

4. Experimental method for constructing Poincaré maps

Even though theoretical and numerical studies of chaotic advection in three-dimensional flows are appearing with increasing frequency in the literature (see Sotiropoulos *et al.* 2001 and Fountain *et al.* 2000 for recent reviews), experimental studies have been strikingly scarce (Fountain, Khakar & Ottino 1998; Fountain *et al.* 2000). The scarcity of experimental work is partly due to the lack of a simple experimental technique for constructing Poincaré maps in the laboratory (Mezić & Sotiropoulos 2002). In fact the first successful attempt to construct experimental Poincaré maps for a chaotically advected three-dimensional flow was reported only recently by Fountain *et al.* (1998, 2000). Fountain *et al.* employed injection needles to deliver small blobs of dye at various locations within the chaotically advected region of their low-*Re* flow and, thus, specify a set of initial 'particle' locations. The intersections of the resulting streaks of dye with a laser sheet constitute, by definition, the Poincaré map of the flow. This technique, however, is cumbersome to implement and is not suitable for general three-dimensional flows – see Fountain *et al.* (2000). Vortex-breakdown bubbles, for instance, are known to be extremely sensitive to small disturbances (see discussion in § 3 above) and, thus, intrusive experimental techniques are not appropriate.

In this work we developed a non-intrusive and simple to implement, experimental technique for constructing Poincaré maps. The technique employs standard planar LIF and can be summarized as follows. At $t = 0$ introduce fluorescent dye with spatially non-uniform concentration within the chaotically advected region of the flow. Assume that the concentration of dye is advected perfectly by the flow (i.e. molecular diffusion effects are negligible) and illuminate a diametral plane with the laser sheet to specify the plane for the Poincaré map. The dye concentration on this plane is related linearly to the intensity of emitted light. Using digital photography, collect a sufficiently long sequence of instantaneous LIF images and superimpose them to compute the (Eulerian) time-average of the light intensity at every point on the diametral plane. The level sets of the resulting time-averaged light intensity field visualize the un-mixed islands of the Poincaré map of the flow. Mezić & Sotiropoulos (2002) presented a formal mathematical proof of this assertion by showing that in a steady flow the local Eulerian time-average of a quantity conserved along particle paths, such as the concentration of fluorescent dye, is equal to the Lagrangian time average of the same quantity along the particle path that passes through that point. Ergodic theory rigorously establishes that as time approaches infinity such a Lagrangian time average exists (see Mezić & Sotiropoulos 2002 for a detailed discussion). This link between Eulerian and Lagrangian time averages places the present experimental technique in the same context as earlier numerical studies in which it was shown that unmixed islands in a chaotically advected flow are found around the extrema of the Lagrangian time-average field (Mezić & Wiggins 1999; Malhotra, Mezić & Wiggins 1999). For more details on the theoretical aspects of the present technique along with its extension to time-periodic flows the reader is referred to Mezić & Sotiropoulos (2002).

There are two prerequisites for successful application of the above technique: (i) the initial spatial distribution of fluorescent dye within the chaotically advected region must be non-uniform; and (ii) the averaging time must be shorter than the molecular

diffusion time scale of the flow but longer than the characteristic time scale of the flow (Mezić & Sotiropoulos 2002). To ensure that an initial non-uniform concentration of dye was trapped in the interior of the bubble, we adopted a technique similar to that used by Escudier (1984) to visualize the third bubble for governing parameters in the steady three-bubble regime. For a given Reynolds number, we ran the experiment long enough to ensure that transients had died out and a steady state had been established. We started the flow of dye at a constant flow rate and as soon as the vortex-breakdown bubble had become visible and a sufficient amount of dye was recirculating within it, we imposed a mild unsteady perturbation by spinning-up (increasing Ω by 2% for 50 lid rotations) and then returning the rotating lid to the desired Re. The ensuing transient flow introduced dye into the core of the bubble or pair of bubbles and resulted in the desired non-uniform spatial distribution of concentration. As soon as the desired rotational speed had been re-established, we allowed the flow to relax to steady state before we commenced the image acquisition procedure. The second prerequisite for the success of the experimental technique is also satisfied in all subsequently reported experiments. A typical image acquisition period is 12 or 24 minutes (see the subsequent discussion) while the diffusion time scale of the dye over the size of an unmixed island is estimated to be approximately one order of magnitude longer. For instance, the diffusion time scale over the cross-sectional dimension of the period-three island for the $Re = 1850$, $H/R = 1.75$ case (see figure 8*c* below) is estimated to be 150 minutes, where the dye diffusivity is $10^{-9}\,\mathrm{m^2\,s^{-1}}$. Note that a 12 minute image acquisition interval is sufficient for visualizing unmixed regions in the flow because, as we will subsequently show, the averages of dye concentration converge very rapidly at points within unmixed islands and other invariant sets (such KAM-tori).

5. Numerical methods

A detailed description of the numerical method we employ to solve the Navier–Stokes equations can be found in Sotiropoulos & Ventikos (1998). Here it suffices to mention that we solve the Navier–Stokes equations in generalized, curvilinear coordinates using a finite-volume approach that is second-order accurate both in space and time. All results presented herein were obtained on a mesh with $153 \times 97 \times 97$ grid nodes in the axial and transverse directions, respectively (see Sotiropoulos & Ventikos 2001 for details of the mesh topology). Systematic grid refinement studies showed that this grid density is sufficient for resolving both the Eulerian and Lagrangian characteristics of the flow (see Sotiropoulos *et al.* 2001). Particle paths were calculated using a fourth-order-accurate Runge–Kutta method in conjunction with a tri-linear spatial interpolation technique. Extensive sensitivity studies were carried out to ensure that the overall Lagrangian features of the flow are insensitive to the size of the time increment used in the trajectory integration. A detailed discussion of these issues can be found in Sotiropoulos *et al.* (2001).

6. Results and discussion

In this section we present the results of our experiments along with additional computational results, which clarify and further reinforce the laboratory findings. Experiments were performed for two aspect ratios ($H/R = 1.75$ and 2) and for a range of Reynolds number in the steady flow regime. We begin our discussion by presenting experimental evidence of the very long chaotic transients in the interior of

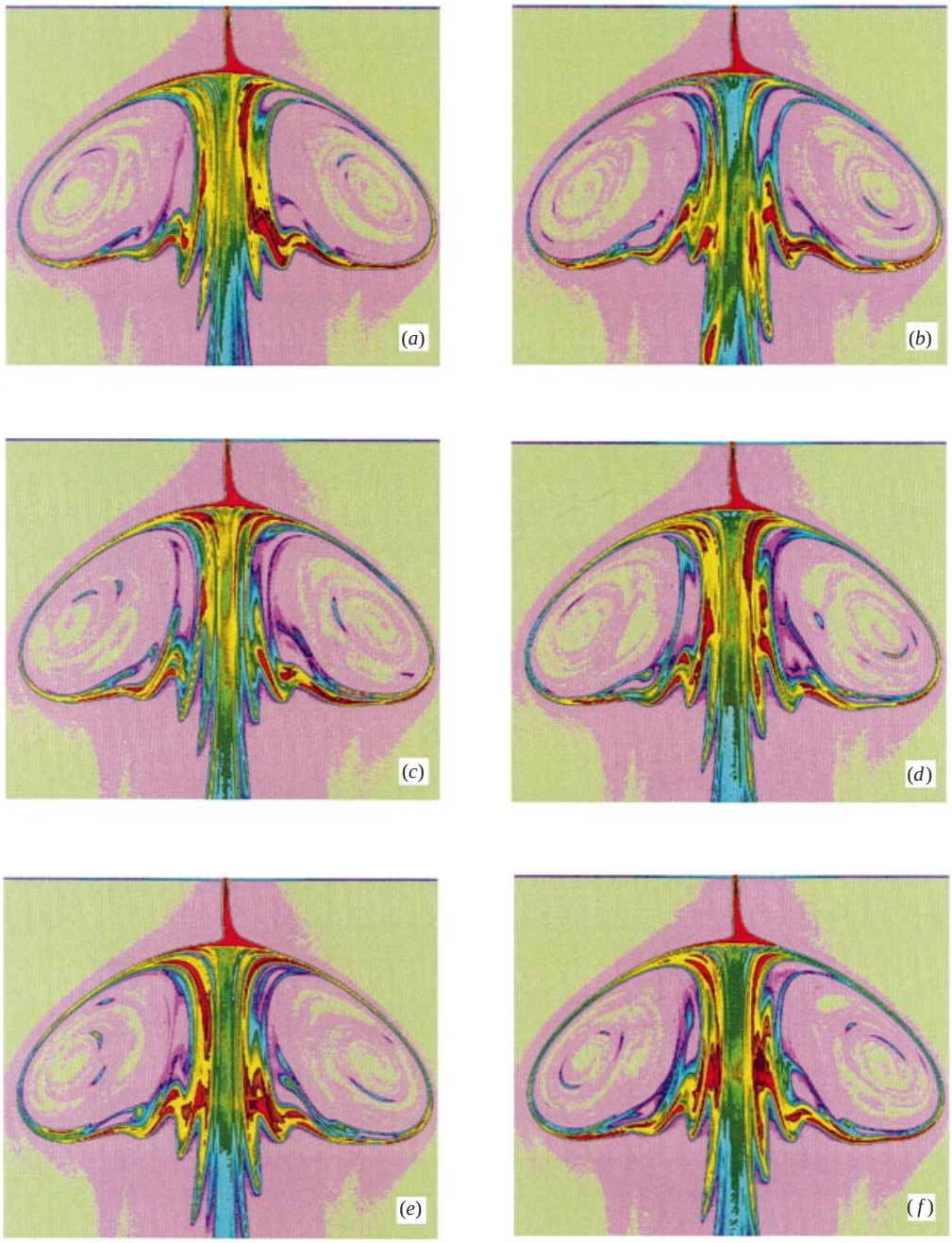

FIGURE 4. Instantaneous iso-contours of light intensity for a steady vortex-breakdown bubble ($Re = 1850$, $H/R = 1.75$). The images shown span an interval corresponding to 400 lid revolutions and are equally spaced in time (time increases from *a* to *f*). Bubble diameter is $0.49R$.

the steady vortex-breakdown bubbles. We also document experimentally the bursting events via which fluid exits the bubble and the very long residence times of dye tracer in the interior of the bubble after the dye supply is interrupted. Subsequently we employ the ergodic visualization method discussed above to construct Poincaré

maps for various Reynolds numbers in the single-bubble regime. Finally, we report results for a steady two-bubble flow and focus on the strikingly simple dynamics of the second bubble.

6.1. *Lagrangian transients in steady vortex-breakdown bubbles*

To document experimentally the complex Lagrangian transients in the interior of steady vortex-breakdown bubbles, we performed a set of visualization experiments (figure 4) keeping the volume flow rate of dye tracer constant and observing its motion within the bubble over very long intervals – typically of the order of several hundred endwall rotations. The spatial and temporal variations of tracer concentration are illustrated by plotting colour contours of the instantaneous light intensity distribution obtained from the LIF technique. In all contour plots shown below, the light intensity is scaled with the maximum light intensity so the levels vary between zero and one.

Figure 4 shows a sequence of instantaneous distributions of light intensity in the interior of the steady vortex-breakdown bubble for $Re = 1850$ and $H/R = 1.75$. Note that due to space considerations we only show herein results for one case. However, all vortex-breakdown bubbles that we have visualized in this work exhibit the same general trends.

There are several important observations that can be made based on the images shown in figure 4. Perhaps the most intriguing feature, and one that has not been previously identified in earlier studies, is that the transport of dye tracer in the interior of the bubble appears to vary in a random and unsteady manner over the entire observation interval. Similarly, the asymmetric folds at the downstream end of the bubble are clearly seen to stretch, albeit very slowly, up and down with time without any signs of reaching a steady state – we have observed vortex-breakdown bubbles over much longer time intervals than the one shown herein and always observed this slow stretching of the folds. A similar slow temporal variation of the folds is also present in the visualization photographs of Spohn *et al.* (1998) (see the sequence of images in figure 10 of their paper). Lagrangian unsteadiness is especially evident within the cylindrical region surrounding the container axis. As discussed in Sotiropoulos *et al.* (2001), this region is occupied by chaotic Šil'nikov orbits that spiral upwards, from the spiral-in to the spiral-out saddles, and then downward along the surface of the bubble. The chaotic stirring of these orbits and the arbitrarily long transients associated with the infinite-period homoclinic orbits are responsible for the random and unsteady motion of dye tracer within this columnar filament.

As shown experimentally in Spohn *et al.* (1998) and subsequently verified and further clarified via numerical computations by Sotiropoulos & Ventikos (2000), the bubble is filled and emptied through the downstream saddle focus – although not shown herein, our experiments confirm the same filling and emptying mechanism as described by Spohn *et al.* (1998). Sotiropoulos *et al.* (2001) further showed that upstream-originating markers that enter the bubble exit in a seemingly random sequence of bursting events during which clusters of markers exit the bubble. They also showed that the rate of decay of an initial population of particles that originated upstream and entered the breakdown region is a devil's staircase distribution. The images shown in figure 4 do suggest that, at least in a broad qualitative sense, this bursting mechanism is indeed at work in steady vortex-breakdown bubbles. Notice for instance that the light intensity at the exit of the bubble is not constant in time but rather varies in a random manner. This seemingly random variation of light intensity is clearly depicted in figure 5, which shows the time series of light intensity at a point on the axis at the exit of the bubble for $Re = 1850$ and $H/R = 1.75$ – the time-series

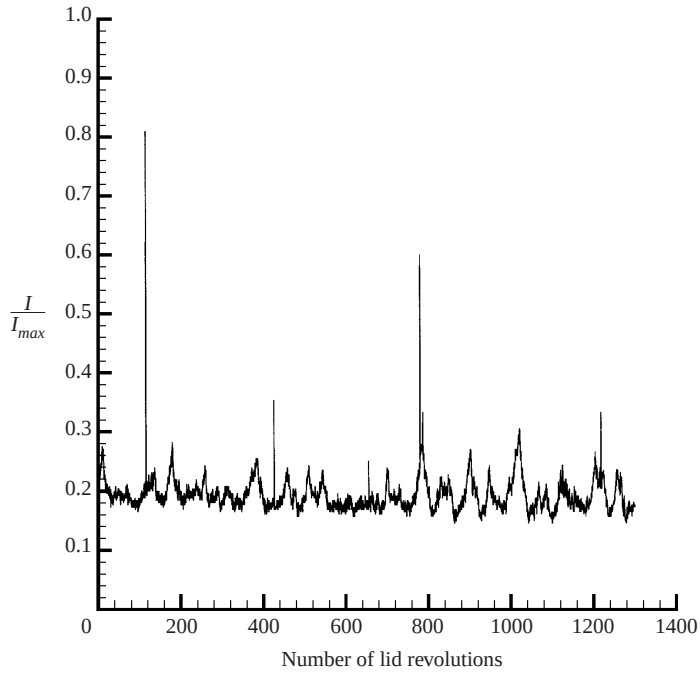

FIGURE 5. Time series of light intensity at a point on the centreline just downstream of the spiral-in saddle of the steady vortex-breakdown bubble for $Re = 1850$, $H/R = 1.75$. The light intensity is normalized by the maximum value I_{max} in the field, which typically occurs at the upstream stagnation point.

data were extracted from the complete sequence of LIF images. It is evident from this figure that there are relatively long time intervals during which the flow of tracer through the spiral-in saddle is reduced to a minimum level. Such intervals correspond to the longer plateaux of the devil's staircase. On the other hand, clusters of distinct spikes in the time series correspond to a series of short plateaux. Figure 5 also reveals that both the waiting time between consecutive bursts (spikes) and the intensity of each burst seem to vary in a random manner.

To document that the location of the bubble is stationary in time in our experiment, we superimpose in figure 6 instantaneous snapshots of a single iso-surface of light intensity over an observation interval of 526 endwall revolutions. It is apparent from this figure that the overall shape and location of the bubble are remarkably stable in time. Unsteady fluctuations of the light intensity are only visible in the interior of the bubble and in the vicinity of the spiral-in saddle. It is important to emphasize once again that the term 'unsteadiness' refers herein to the Lagrangian transport. For all Reynolds numbers we have studied in this work the flow is steady from the Eulerian standpoint and experimental evidence in support of this assertion is provided in figure 6. The fact that the tracer motion is steady upstream of the bubble strongly suggests that the approach flow is steady (from the Eulerian standpoint) as well. Of course, one may argue that the apparent unsteadiness of tracer transport within and downstream of the bubble could be due to flow unsteadiness within the bubble. Since this is a closed recirculating flow system, however, unsteady Eulerian modes excited within the vortex-breakdown bubble would affect the flow throughout the entire container and, thus, would manifest themselves in the tracer

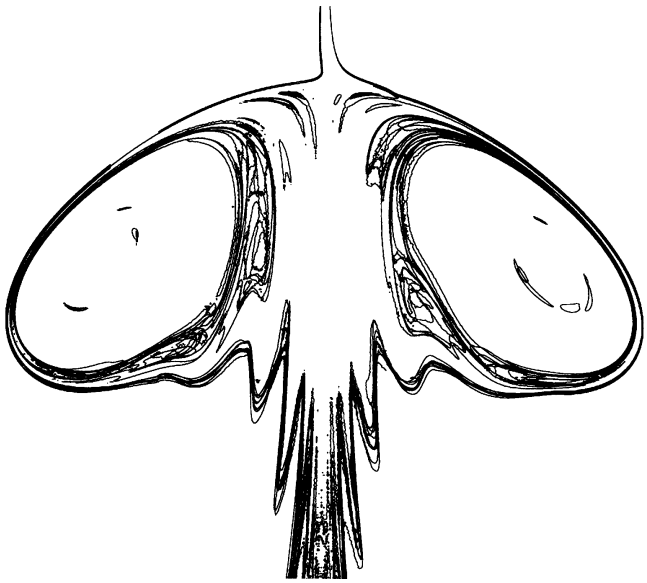

FIGURE 6. An iso-surface of light intensity plotted at various instants in time for a steady vortex-breakdown bubble. $Re = 1850$, $H/R = 1.75$, $I/I_{max} = 0.35$. The observation interval corresponds to 526 lid revolutions and the iso-surface is plotted every 36 revolutions. Different lines correspond to different instants in time. Bubble diameter is $0.49R$.

motion upstream of the bubble as well. This argument is not, by itself, conclusive enough to establish the steadiness of the flow with absolute certainty. This issue is very important in the context of the present work since, as we have already discussed above, even an arbitrarily small unsteady mode could drastically alter the Lagrangian properties of the flow (Holmes 1984). Recall, however, that our experimental results are corroborated by our earlier numerical computations. In Sotiropoulos *et al.* (2001) we showed that in a steady-state velocity field residence times of upstream-originating particles within the breakdown region could be very long and that their spatial distribution, when mapped to upstream initial conditions, exhibits very complex fractal properties. In fact, we found that as the spatial density of initial conditions increases, initial conditions leading to progressively higher residence times are continuously being uncovered. For example, at the finest resolution we employed in Sotiropoulos *et al.* (2001) we found initial conditions that remained within the bubble for nearly 3000 lid rotations (approximately 60 minutes of dimensional time for our experimental apparatus). Arbitrarily long Lagrangian transients may indeed be expected in the laboratory because the time that is required for a steady Lagrangian image to be obtained is equal to the maximum residence time for a fixed set of upstream initial conditions and constant volume flow rate of markers originating from this set.

6.2. *Residence times*

To document experimentally the very long residence times of dye tracer within the vortex-breakdown region, we performed an experiment aimed at quantifying the rate at which a fixed amount of tracer, initially in the interior of bubble, decays in time. The experiment was conducted as follows. First we set the rotational speed of the lid to the desired Reynolds number and allowed sufficient time for the flow to reach steady state. Subsequently we started releasing fluorescent dye to visualize the flow and continued the supply of dye for approximately 100 lid revolutions to ensure that

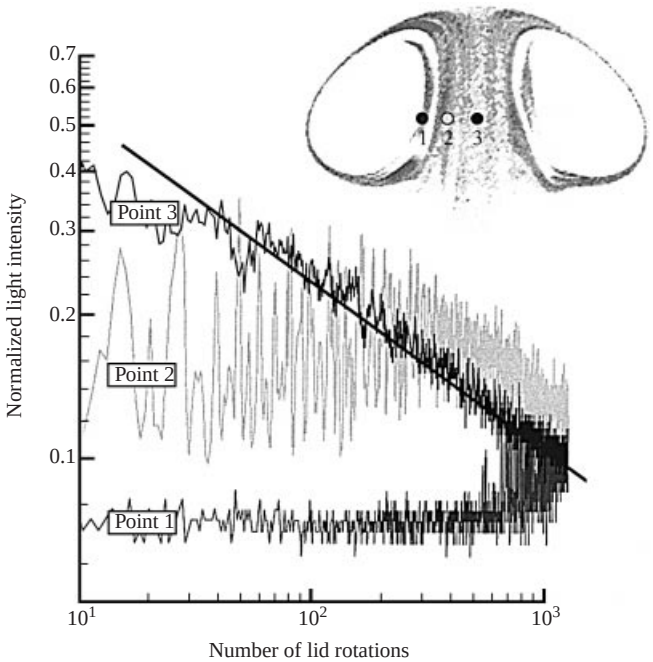

FIGURE 7. Time series of light intensity recorded after the dye supply was interrupted ($t = 0$) at three points (see sketch for the locations) in the interior of the steady vortex-breakdown bubble for $Re = 1850$, $H/R = 1.75$.

a sufficient amount of dye had entered the bubble. At that point, we interrupted the supply of dye and started the data acquisition process. We recorded LIF images over a time interval corresponding to 1300 lid revolutions. It is important to note that no special attempt was made during this experiment to trap dye within the internal toroidal region of the bubble using the previously described transient perturbation technique.

Figure 7 depicts time series of light intensity at three pixels of the digital image in the interior of the vortex-breakdown bubble for $Re = 1850$ and $H/R = 1.75$. The specific points were selected because their respective time series are representative of the various trends we recorded throughout the bubble. It is evident from this figure that these trends vary significantly in different regions of the bubble and this is to be expected given the richness and complexity of the dynamics. At the innermost point, point 1 in figure 7, the light intensity remains at a low level for a very long time but it starts increasing rapidly after approximately 1000 lid revolutions. As we have already discussed above, in this experiment we made no attempt to trap dye in the interior of the bubble. Thus, the blobs of tracer that arrived at point 1 after 1000 lid revolutions have been transported there along upstream-originating orbits that penetrated the internal toroidal region. Recall that according to the numerical results of Sotiropoulos *et al.* (2001), the innermost core of this toroidal region is foliated with regular KAM-tori. This impermeable core is surrounded by nested cantori and periodic islands submerged within stochastic regions. Particles introduced just outside the outermost KAM-torus were shown by Sotiropoulos *et al.* (2001) to escape through the cantori and exit the bubble. Since the flow is incompressible, the volume of the bubble that is accessible to upstream-originating particles must be equal to its total

volume minus the volume occupied by KAM-tori and unmixed islands (see related discussion in MacKay 1994). Clearly, therefore, a subset of the total amount of tracer that was in the bubble at $t = 0$ (when the dye supply was interrupted) will have to reach the impermeable toroidal core before it starts moving again toward the axis on its way to exit the bubble. The time series at point 1 in figure 7 suggests that this process could require extremely long times, in fact much longer than the 1300 lid revolutions interval for which we ran this experiment.

The light intensity at point 2 in figure 7 oscillates about a more or less constant mean for almost 400 lid revolutions before it starts decaying. This trend suggests the presence of a cantorus in the vicinity of this point. Orbits may be trapped on such a leaky barrier for very long times and that could account for the long time interval of oscillatory variation around a constant mean. Eventually, however, orbits would start escaping, thus causing the observed temporal decay of light intensity at this point. At point 3, which is located on the axis, the light intensity record starts to decay after a rather short initial transient. As seen in figure 7, after approximately 100 lid revolutions the signal decays according to what appears to be a power law distribution. We should note that we examined time series at several points between points 2 and 3 (see figure 7) and found a similar power-law behaviour. In fact the exponent of the power law seems to be the same for all points in this region. Notice that even at point 2 when the light intensity starts to decay it appears to follow the same power law. This apparent self-similarity and the power-law behaviour should be attributed to the fractal Cantor-set-like structure of the leaky and sticky cantori through which tracers must pass to exit the bubble (MacKay, Meiss & Percival 1984).

Although figure 7 shows temporal variations over an interval corresponding to 1300 lid revolutions (24 minutes), we have observed in the laboratory vortex-breakdown bubbles for much longer time intervals (of the order of several thousands of lid revolutions) and found that the inner toroidal region of the bubble remains visible for extremely long times (of the order of hours, after the dye supply is interrupted). These observations along with our previous discussion provide the first experimental verification of the theoretical and computational predictions concerning the arbitrarily long residence times of upstream-originating tracers within steady vortex-breakdown bubbles.

6.3. *Experimental Poincaré maps: Reynolds number and aspect ratio effects*

Although the instantaneous LIF images discussed in the previous section are broadly consistent with the computational findings of Sotiropoulos *et al.* (2001), they do not provide the kind of information needed for direct quantitative comparisons with the numerical calculations. Given the rich dynamics in the interior of vortex-breakdown bubbles, such comparisons between computations and experiments can only be carried out in terms of Poincaré maps. In this section we construct experimental Poincaré maps using the ergodic visualization technique described in § 4 above. We present results for two aspect ratios ($H/R = 1.75$ and 2) and various Reynolds numbers in the steady flow regime. All experimental maps presented herein were constructed by averaging a sequence of instantaneous LIF images collected over an interval of 12 minutes under a continuous supply of dye at constant flow rate. For all cases, the time-averaged light intensity field is scaled by the maximum light intensity that typically occurs just upstream of the spiral-out saddle focus where the on-axis filament is deflected off the axis. The invariant sets of the Poincaré map of the flow (unmixed island chains) are visualized by plotting the level sets of the averaged light intensity field. Issues related

to the length of the averaging interval needed for obtaining statistically converged results are addressed in detail toward the end of this subsection.

Figure 8 depicts the experimental Poincaré maps for four Reynolds numbers for a container with $H/R = 1.75$. In spite of the anticipated quantitative differences due to Reynolds number effects, all four maps reveal broadly similar dynamics. The uniformly coloured columnar filament along the axis in the interior of the bubbles visualizes the 'Šil'nikov filament' (see Sotiropoulos *et al.* 2001) that connects the spiral-in and spiral-out saddles. Efficient mixing of dye tracer in this filament results in the observed nearly homogeneous distribution of the time-averaged light intensity. According to the numerical Poincaré maps reported in Sotiropoulos *et al.* (2001), particle paths in the internal toroidal region of the bubble exhibit a rich mixture of regular and chaotic dynamics. The experimental maps suggest a similar complexity level. For all four cases, for instance, the internal toroidal region is foliated by nested tori, which could be either KAM-tori or cantori. Based on the numerical results of Sotiropoulos *et al.* (2001), invariant KAM-tori persist in the innermost region of the bubble, which for all cases shown in the figure has been penetrated by small amounts of dye. Another important feature of the dynamics that appears to vary with Reynolds number is the number and period of unmixed islands that emerge within the chaotic regions. For the $Re = 1350$ case, for instance, there is only one period-two island. For $Re = 1600$ (figure 8*b*), on the other hand, another period-two island chain and a period-four island chain have formed. The complexity of the dynamics is seen to further increase at $Re = 1850$, where period-two, period-three and period-four island chains have clearly formed. The numerical computations of Sotiropoulos *et al.* (2001) for this Reynolds number and aspect ratio (see figure 11 in Sotiropoulos *et al.* 2001) are in excellent agreement with the image shown in figure 8(*c*), with regard to both the period and relative location of the island chains. For the highest Reynolds number, shown in figure 8(*d*) ($Re = 2100$), the period-two island is no longer present but the period-three and period-four chains persist.

Poincaré maps for a container with $H/R = 2$ are shown in figures 9(*a*) and 9(*b*) for $Re = 1492$ and 1900, respectively. The latter Reynolds number is, for this aspect ratio, within the two-bubble regime and a second steady vortex-breakdown bubble exists downstream of that shown in figure 9(*b*). An instantaneous LIF image of the two-bubble structure is shown in figure 10 while the dynamics of the second bubble is discussed in the next subsection. For the $Re = 1492$ case there are no unmixed islands in the interior of the bubble and this result is in accordance with the numerical predictions of Sotiropoulos *et al.* (2001). Note that the four red marks along the outer edge of the bubble in figure 9(*a*) mark the intersections of the upstream columnar filament as it is deflected off the axis and spirals toward the spiral-in saddle (see extensive discussion in Sotiropoulos & Ventikos 2001). For the $Re = 1900$ case (figure 9*b*), a clearly defined period-two island has emerged and other higher-period islands may also be present in the region between the period-two island and the columnar filament along the axis (see the several red marks in that region).

An important issue that needs to be addressed in the context of our ergodic visualization technique is with regard to the time interval over which data needs to be collected in order to obtain statistically converged results. This is obviously a critical issue since if excessive times are required for obtaining converged time-averaged values, molecular diffusion could begin to smear the spatial gradients of the light intensity field. As shown in Mezić & Sotiropoulos (2002), convergence within low-period invariant tori should be very rapid. To demonstrate this theoretical argument, we show in figures 11 and 12 the spectra of the experimental time series

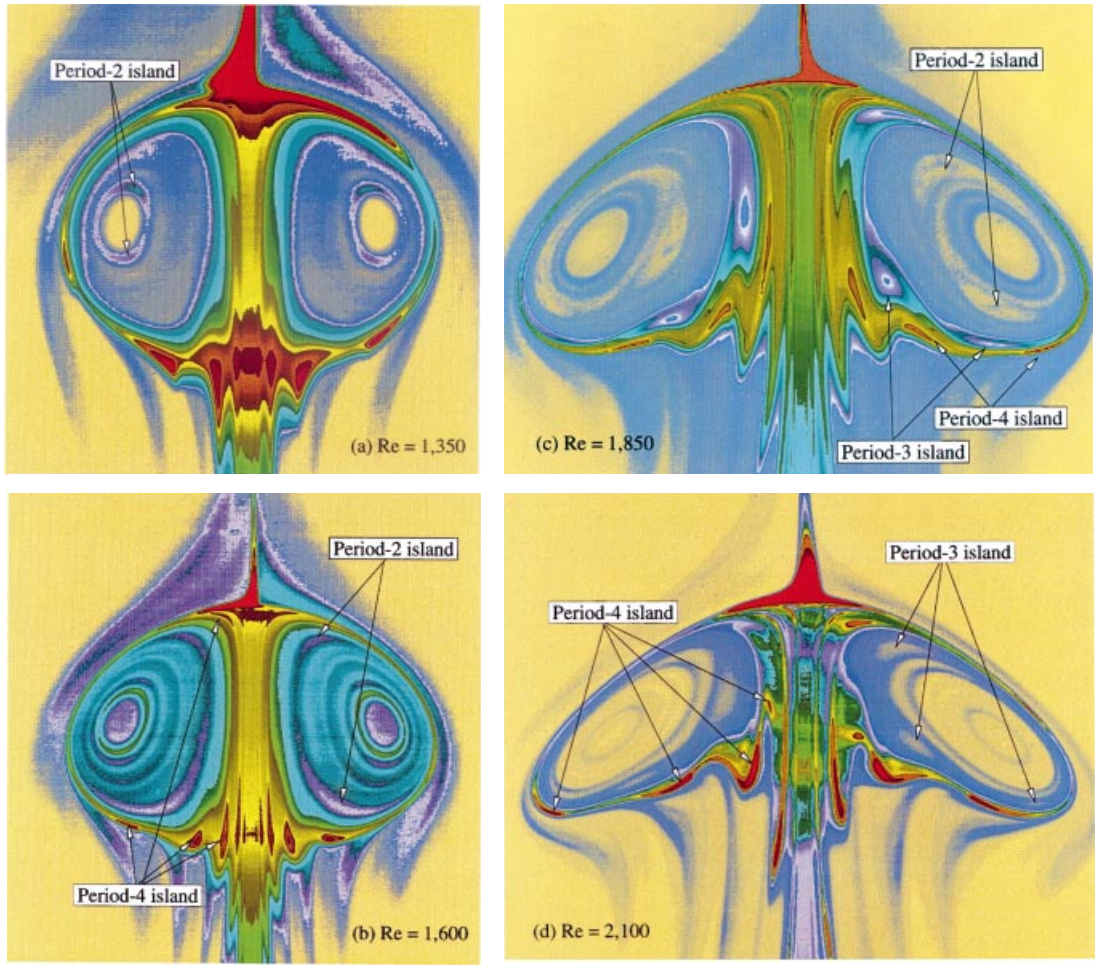

FIGURE 8. Experimental Poincaré maps for steady vortex-breakdown bubbles in a container with $H/R = 1.75$: (*a*) $Re = 1350$, bubble diameter is $0.23R$; (*b*) $Re = 1600$, bubble diameter is $0.44R$; (*c*) $Re = 1850$, bubble diameter is $0.49R$; (*d*) $Re = 2100$, bubble diameter is $0.50R$.

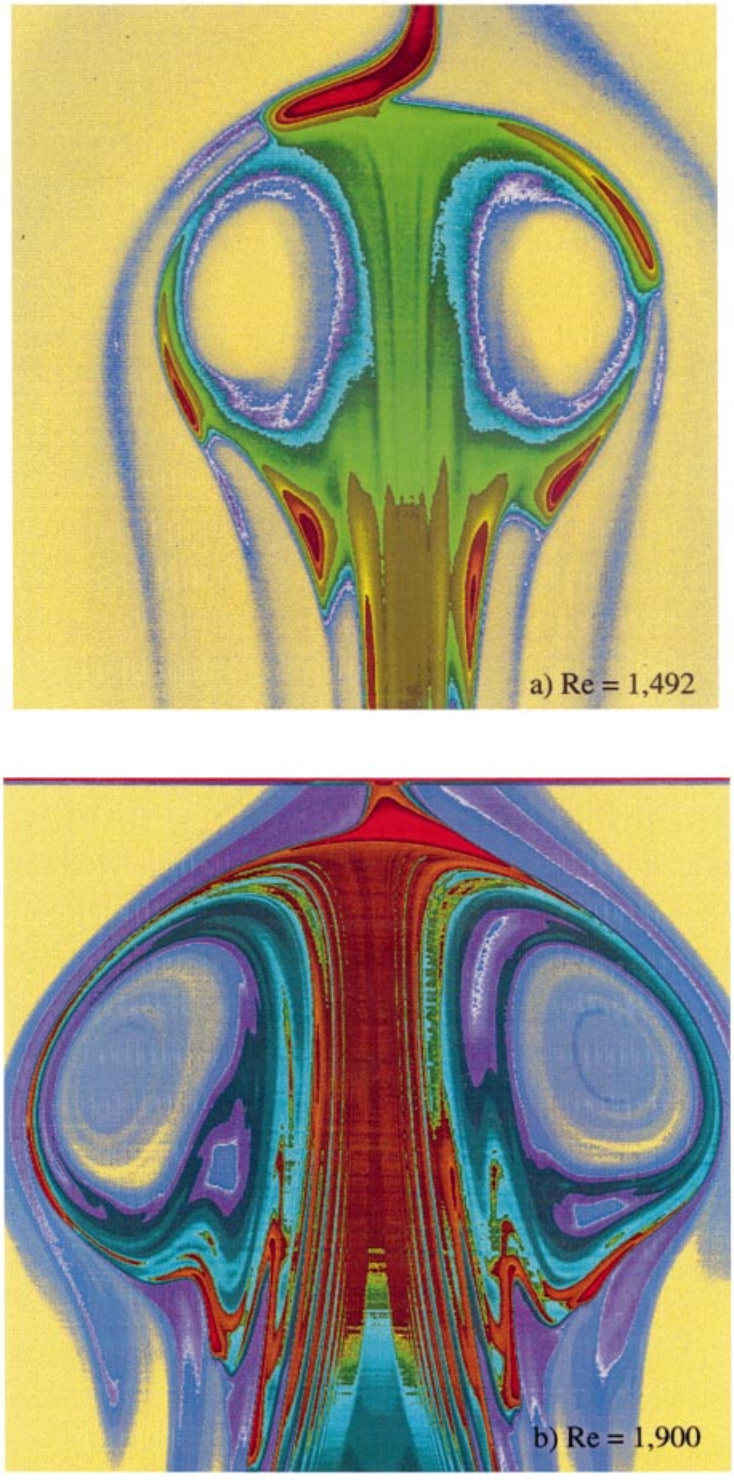

FIGURE 9. Experimental Poincaré maps for steady vortex-breakdown bubbles in a container with $H/R = 2.0$: (*a*) $Re = 1492$, bubble diameter is $0.21R$; (*b*) $Re = 1900$, first bubble diameter is $0.48R$.

FIGURE 10. Visualized steady vortex-breakdown bubbles for $H/R = 2.0$ and $Re = 1900$, first bubble diameter is $0.48R$.

of light intensity and the convergence history of the average of the light intensity, respectively, at three points within the vortex-breakdown bubble shown in figure 9(b). The first point is placed on the axis within the chaotic Šil'nikov filament, the second point is placed within the period-two island, and the third point is within the innermost toroidal region that is occupied by quasi-periodic orbits. The broadband spectrum shown in figure 11(a) is consistent with the chaotic stirring of orbits within the Šil'nikov filament. As seen in figure 12(a), the time-averaging procedure appears to converge very slowly and this is in accordance with the existence of arbitrarily long Šil'nikov transients in this region. The spectra shown in figures 11(b) and 11(c), on the other hand, suggest two-frequency quasi-periodicity as, for each case, all significant peaks are integer-linear combinations of the two fundamental frequencies, f_1 and f_2. The quasi-periodicity of the light-intensity time series is consistent with the quasi-periodic dynamics of particle paths moving along two-tori in the innermost toroidal region and the period-two regular island, respectively. As seen in figure 12, the time-averaging procedure at such points converges very rapidly, typically within 100 lid rotations. Even though we have only included results for one vortex-breakdown bubble and at few representative points, examination of other data sets leads to the same conclusion, namely that statistically converged results are obtained very rapidly

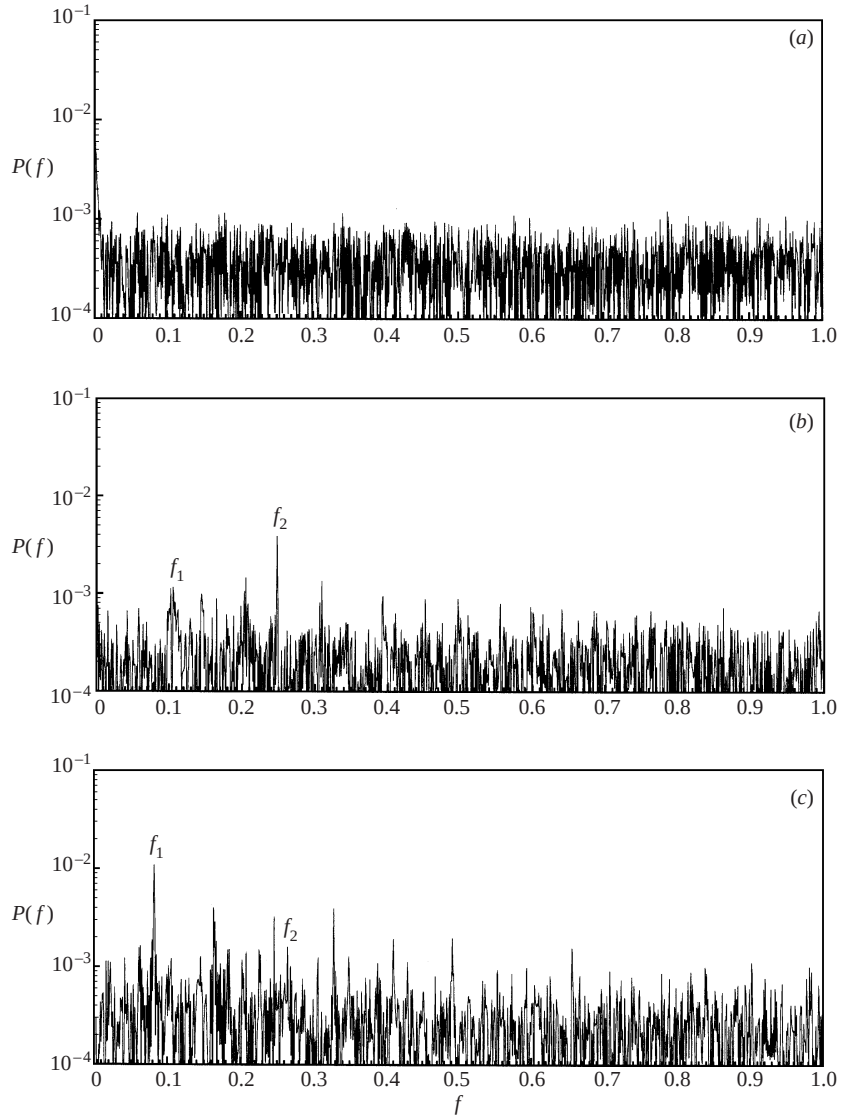

FIGURE 11. Power spectra of light-intensity time series at three points within the first vortex-breakdown bubble for $Re = 1900$, $H/R = 2$ (under continuous supply of dye at a constant flow rate). The points are located (*a*) on the axis; (*b*) inside the period-2 island; and (*c*) within the internal, quasi-periodic, toroidal region (see figure 9*b*).

within areas of regular motion (quasi-periodic period-one tori and higher-period unmixed islands). Since, therefore, the aim of our ergodic experimental technique is to identify regular islands of the flow, the above results show that statistically converged invariant sets of Poincaré maps can indeed be obtained within time intervals far shorter than the molecular diffusion time scale (see Mezić & Sotiropoulos 2002 for a detailed discussion).

6.4. *The dynamics of the second bubble in the steady two-bubble regime*

As was first shown experimentally by Escudier (1984), there is a range of governing parameters within which two or even three steady vortex-breakdown bubbles can form

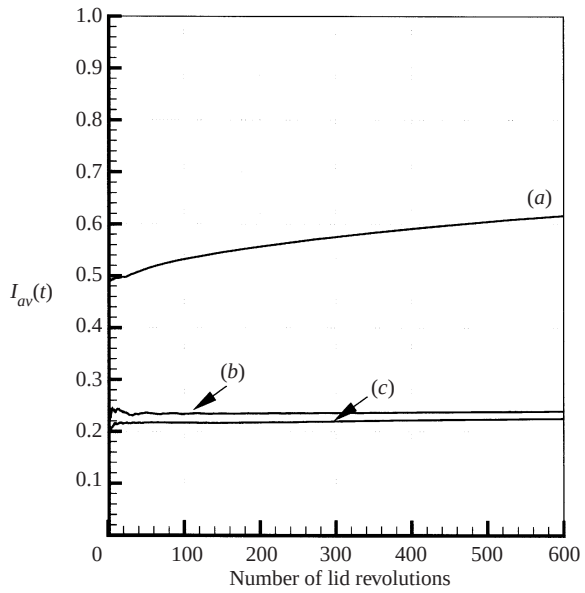

FIGURE 12. Temporal convergence of the time average of light intensity $I_{av}(t) = (1/t)\int_0^t I(t')\,dt'$ for the three points of figure 11.

along the container axis. The two-bubble structures visualized by Escudier (1984), which are very similar to the structure shown in figure 10, reveal that the first and the second bubble have distinctly different features, with the latter appearing to be almost perfectly axisymmetric and closed. It is evident in Escudier's photographs that, unlike the first bubble, very little dye penetrates the interior of the second bubble. In this section we examine experimentally and computationally the Lagrangian dynamics of the second bubble and identify the reasons for these apparent structural differences between the two bubbles. In § 7 we show that these differences are due to the different levels of swirl characterizing the two bubbles.

Figure 13 shows representative instantaneous iso-contours of light intensity over a time interval spanning 600 lid revolutions. It is evident from this sequence of images that the light intensity within the bubble varies continuously with time in a manner similar to that observed for the chaotic vortex-breakdown bubble in figure 4. Plotting iso-contours of the time-averaged light intensity field (figure 14), however, yields an image which exhibits a high degree of symmetry with respect to the axis, in stark contrast with the Poincaré maps for chaotic bubbles (see figure 9 above). The interior of the bubble for this case is seen to be foliated by a sequence of nested toroidal iso-surfaces of light intensity – the wiggles on some of the iso-contours are due to slight variations in the light intensity of the laser sheet, which result from the laser beam itself as well as slight irregularities in the Plexiglas container. The remarkable symmetry of the experimental image appears to suggest that the dynamics of the second bubble is fundamentally different from that of the first one and that characterizing vortex-breakdown bubbles in the single-bubble regime.

To identify the reasons for the symmetry of the experimental map shown in figure 14, we show in figure 15 the calculated Poincaré map for the second vortex-breakdown bubble for $Re = 1900$ and $H/R = 2$. As seen in the computed map, orbits in the interior of this bubble move along quasi-periodic, invariant tori. That is, the second vortex-breakdown bubble exhibits essentially the same dynamics as the unperturbed

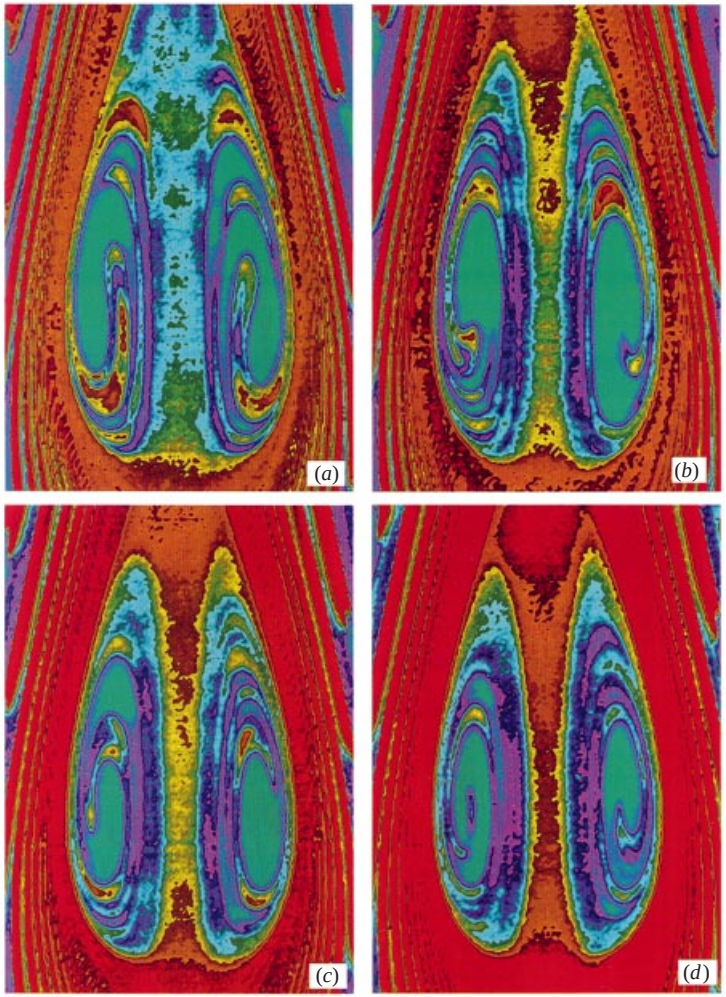

FIGURE 13

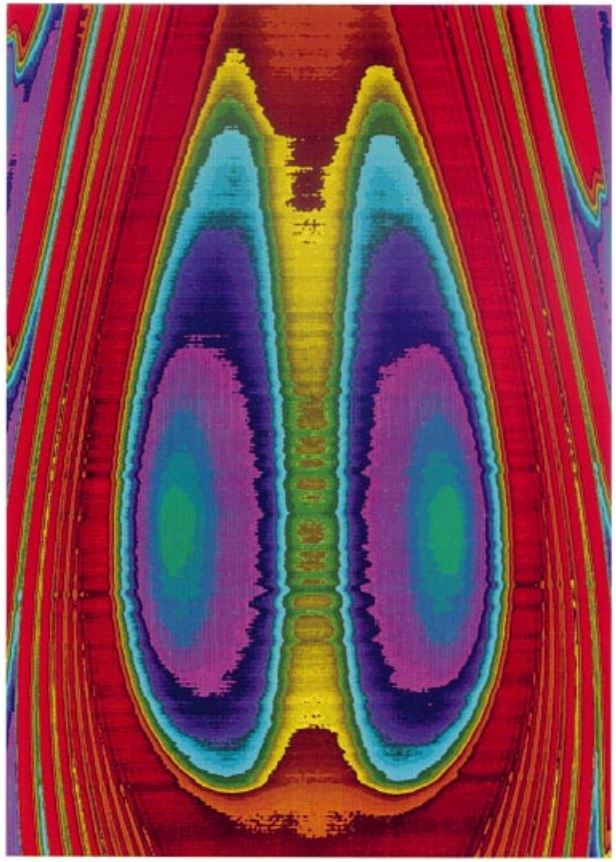

FIGURE 14

FIGURE 13. Instantaneous iso-contours of light intensity within the second vortex-breakdown bubble for $Re = 1900$, $H/R = 2$, second bubble diameter is $0.11R$. The images shown span an interval corresponding to 600 lid revolutions (time increases from a to d).
FIGURE 14. Experimental Poincaré map for the second vortex-breakdown bubble for $Re = 1900$, $H/R = 2$, second bubble diameter is $0.11R$.

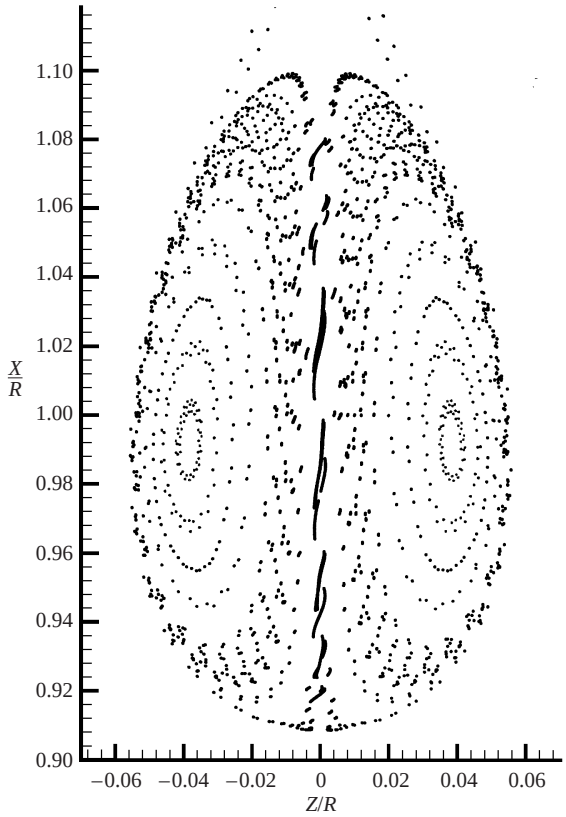

FIGURE 15. Calculated Poincaré map for the second vortex-breakdown bubble for $Re = 1900$, $H/R = 2$.

axisymmetric flow, even though for both the first and second bubbles the velocity field is subject to the same level of three-dimensional disturbances.

It is important to note that the quasi-periodicity of the second bubble is entirely consistent with the long transients of dye tracer suggested by the instantaneous LIF images shown in figure 13. An integrable vortex-breakdown bubble would in general be foliated by invariant two-tori whose rotation number could be either rational or irrational. For rational tori, particles move along periodic orbits and will eventually re-visit their initial location – even though for high-period tori very long times may be required for this to occur. For irrational tori, on the other hand, orbits will cover ergodically the entire torus, coming arbitrarily close to, but never exactly re-visiting, their initial position. Such tori would exhibit infinitely long transients and along with the very long transients of high-period rational tori would account for the apparent unsteadiness of the dye tracer in the experimental images.

To demonstrate the quasi-periodic dynamics of the second bubble experimentally, we show in figure 16 the power spectra of the light-intensity time series at three points within the bubble: one on the axis and two in the interior. For the two inner points the signals exhibit clear quasi-periodic variations while the on-axis signal is chaotic. Although not shown herein, we have found that there is a cylindrical region around the axis within which time series of light intensity exhibit similar chaotic characteristics. For points sufficiently far from the axis we have consistently obtained quasi-periodic

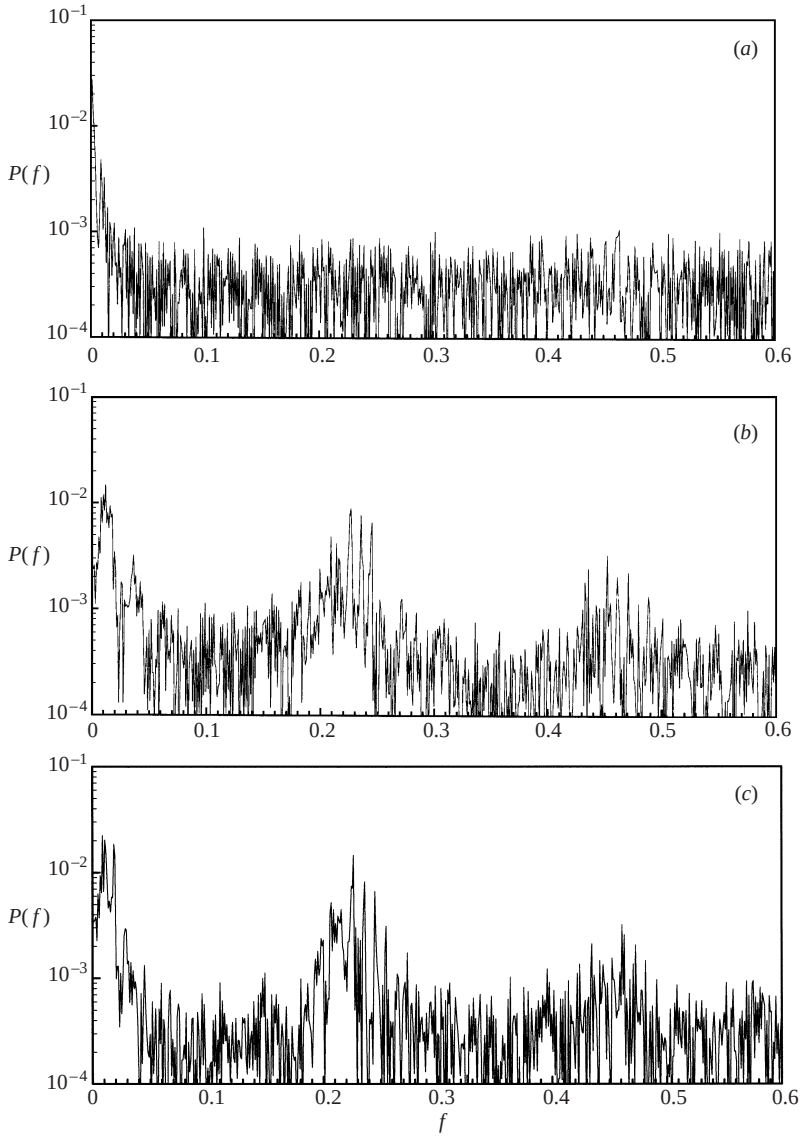

FIGURE 16. Power spectra of light intensity at three points within the second vortex-breakdown bubble for $Re = 1900$, $H/R = 2$ (under continuous supply of dye at a constant flow rate: (*a*) $r/r_b = 0$, (*b*) $r/r_b = 0.33$, (*c*) $r/r_b = 0.39$). All three points are located at the same axial location (at the bubble half-length): (*a*) on the axis; and (*b*) and (*c*) within the internal toroidal region (r_b is the maximum radial thickness of the bubble).

signals such as those shown in figure 16(*b*, *c*). Given the regular structure of the computed Poincaré map in the vicinity of the axis (see figure 15), the reason for the chaotic light-intensity signal in figure 16(*a*) is not readily apparent.

To explain this behaviour, we show in figure 17 the calculated trajectory of a single particle initially placed within the first bubble. The particle recirculates for several time units within the bubble, exits through the spiral-in saddle, spirals around the second bubble, and enters it through its downstream end. When inside the second bubble such orbits recirculate for several time units, spiralling upward along the

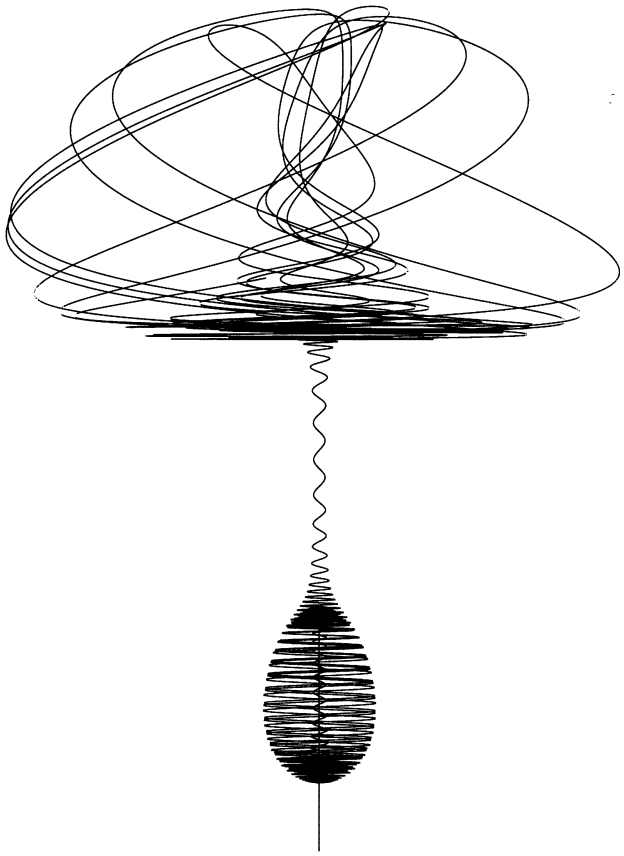

FIGURE 17. Calculated orbit of a single particle starting within the first vortex-breakdown bubble for $Re = 1900$, $H/R = 2$. The orbit recirculates for several time units within the first bubble, then exits and enters the second bubble through its downstream end.

axis and then downward on the surface of the bubble and eventually exit without penetrating the internal toroidal region. It is important to emphasize that even though these orbits move in a manner similar to the Šil'nikov orbits in the first bubble, they do not develop extreme sensitivity to initial conditions, as is evident from the calculated Poincaré map shown in figure 15 – also see § 7 below.

Based on the trajectory shown in figure 17 and the computed Poincaré map shown in figure 15, the second vortex-breakdown bubble can be described as an elongated (egg-shaped) toroidal region, centred around the axis, within which orbits move along nested quasi-periodic invariant tori. The cylindrical core of this toroidal structure is occupied by upward-spiralling orbits, which originate upstream, enter the bubble through its downstream end, and recirculate around the invariant toroidal region for several time units before they finally exit through the downstream spiral-in saddle. Many of these orbits, however, have previously visited the first bubble and, thus, been chaotically stirred. In other words, in the experiment dye tracer enters the cylindrical core of the second bubble at a rate that is determined by the random bursting events via which tracer exits from the first bubble. That is, the chaotic time series shown in figure 16(a) is not the manifestation of chaotic dynamics within the second bubble but rather the signature of the chaotic outflow of tracer from the first bubble.

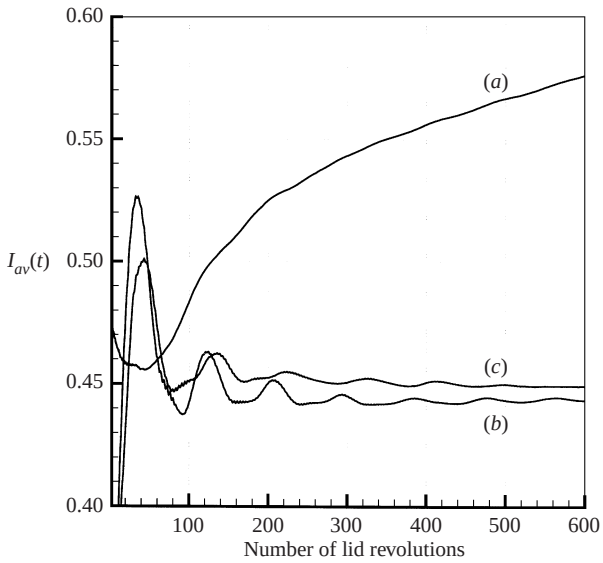

FIGURE 18. Temporal convergence of the time-average of light intensity for the three points in figure 16.

Finally, the convergence of the time-averaged light intensity for the second bubble is illustrated in figure 18. Once again, it is obvious that the averaging process converges very rapidly (within 200 to 300 lid rotations) at points located on invariant quasi-periodic tori, while the convergence of the chaotic time series on the axis is very slow.

7. Dynamical bifurcations of vortex-breakdown bubbles: the role of swirl intensity

In this section we study the bifurcations of a simple dynamical system with phase-space dynamics strikingly similar to the Lagrangian dynamics of real-life steady vortex-breakdown flow fields. This system is the normal form studied theoretically by Broer & Vetger (1984) and discussed in Wiggins (1990) – see also the detailed discussion in Sotiropoulos *et al.* (2001). We select the various coefficients in this normal form to ensure that the transporting velocity field is divergence-free (volume preserving case). We also modify the equations by introducing a steady three-dimensional perturbation field. The perturbation field we (arbitrarily) chose herein is a mode-2 azimuthal disturbance in the axial velocity component and is designed to ensure that the perturbed system also remains volume preserving. The system we study herein is

$$\frac{\mathrm{d}x}{\mathrm{d}t} = 0.04 - r^2 - x^2 + \epsilon r^3 \sin(2\theta), \quad \frac{\mathrm{d}r}{\mathrm{d}t} = rx, \quad \frac{\mathrm{d}\theta}{\mathrm{d}t} = \omega, \tag{7.1}$$

where ω is the angular velocity and ϵ is the parameter that controls the level of the non-axisymmetric perturbation. We should point out that the velocity field in the above equations does not satisfy the Navier–Stokes equations. It is, therefore, important to emphasize that, unlike in previous studies of chaotic advection in which particle path dynamics were studied using analytical solutions of the Navier–Stokes equations (e.g. Stone, Nadim & Strogatz 1991; Ashwin & King 1997; Kroujiline & Stone 1999), here we are only interested in the solutions of (7.1) to the extent

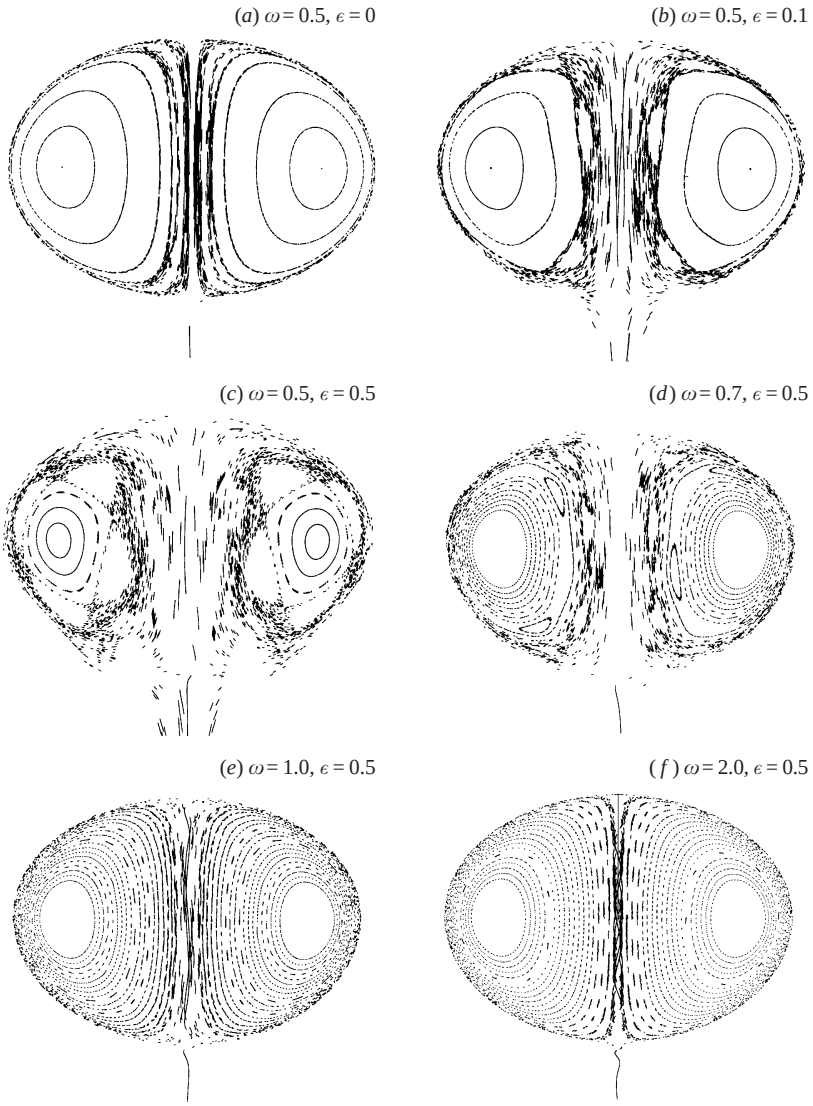

FIGURE 19. Poincaré maps for the system given by equations (7.1) for various levels of perturbation strength ϵ and swirl intensity ω.

that their dynamics is qualitatively similar to that of real-life vortex-breakdown flow fields. In particular, we seek to understand the effect of ω and ϵ on the dynamics of system (7.1) and, guided by this understanding, identify the key Eulerian quantity that governs the dynamics of real-life vortex-breakdown flow fields and propose an explanation for our experimental and computational findings. We compute the orbits of system (7.1) and construct Poincaré maps for various ω and ϵ values (see figure 19). For all cases shown in figure 19, the particle paths were calculated using the same numerical method, the same time-increment, and a velocity field discretized on the same computational mesh – a Cartesian $51 \times 51 \times 51$ box containing the bubble was used as the computational domain.

In the context of vortex-breakdown flows, the first set of computations (figures 19*a* to 19*c*) can be thought as corresponding to an experimental situation where controlled

asymmetric disturbances are introduced into the flow for a fixed Reynolds number (defined by the axial velocity field) and swirl parameter (the ratio of azimuthal to axial velocity components, determined by ω). The second set of computations (figures 19*d* to 19*f*) is aimed at investigating the effect of varying the swirl parameter while keeping the Reynolds number constant within the same experimental apparatus (fixed ϵ). Of course this analogy is more relevant to vortex-breakdown experiments in open systems, where one can vary both the Reynolds number and swirl number independently (Sarpkaya 1971*a*, *b*). For the container problem there is only one control parameter (the lid rotational speed), which determines both the Reynolds number and the swirl parameter.

For the unperturbed ($\epsilon = 0$) $\omega = 0.5$ case shown in figure 19(*a*), the bubble shape appears perfectly axisymmetric (no asymmetric folds) and the internal toroidal region is foliated by invariant KAM-tori. A small stochastic region is seen to exist around the axis but this should be attributed to numerical chaos due to disturbances introduced by the trajectory integration scheme. Note that it was not possible to eliminate this small stochastic region even when we reduced the time step by one order of magnitude. This finding is consistent with the theoretical analysis of Broer & Vetger (1984) who showed that exponentially small disturbances could be sufficient to break the invariance of the bubble, leading to infinite-period orbits homoclinic to the two saddles and the onset of Šil'nikov chaos.

Figures 19(*b*) and 19(*c*) depict the effect of increasing ϵ as ω is held fixed ($\omega = 0.5$). For $\epsilon = 0.1$, the invariance of the bubble has broken and folds, similar to those observed in the laboratory and the numerical simulations of vortex-breakdown bubbles, have formed at the spiral-in saddle focus. The stochastic cylindrical region around the axis has grown significantly and periodic islands have formed within the chaotic region. The internal toroidal region has shrunk compared to the $\epsilon = 0$ case, but invariant KAM-tori still survive. Increasing the perturbation further (figure 19*c*) leads to very pronounced folds and periodic islands of larger cross-sectional area. Invariant tori are still present near the core, but the overall size of this integrable toroidal region has shrunk considerably.

The Poincaré maps shown in figures 19(*d*) to 19(*f*) illustrate the effect of increasing the swirl intensity for the same ϵ. Note that since the asymmetric perturbation is only introduced in the axial velocity field, the axial and radial velocity components are identical for all the maps shown in these figures. That is, from an Eulerian standpoint, the only difference between the three flow fields is the magnitude of the angular velocity ω. As seen in figures 19(*c*) and 19(*d*), increasing the swirl velocity from 0.5 to 0.7 increases the size of the toroidal invariant region, reduces the cross-sectional area of the islands, and nearly eliminates the asymmetric folds. As the swirl intensity is increased to $\omega = 1.0$, the chaotic Šil'nikov column around the axis shrinks to a very thin cylindrical region and eventually disappears completely for $\omega = 2.0$. The bubbles shown in figures 19(*e*) and 19(*f*) are foliated by periodic and quasi-periodic invariant tori and characterized by an entirely axisymmetric shape.

These computations lead to the striking conclusion that even though the velocity field can be three-dimensional, at sufficiently high swirl velocities the Lagrangian dynamics are identical to those of the unperturbed, axisymmetric flow. High swirl velocities have a profound stabilizing effect on the Lagrangian dynamics in a manner that is reminiscent, at least in a qualitative sense, of the stabilizing effect that strong rotation has on Eulerian turbulence.

The bifurcations of this simple dynamical system suggest explanations for a number of our experimental and computational findings. As we have already discussed above

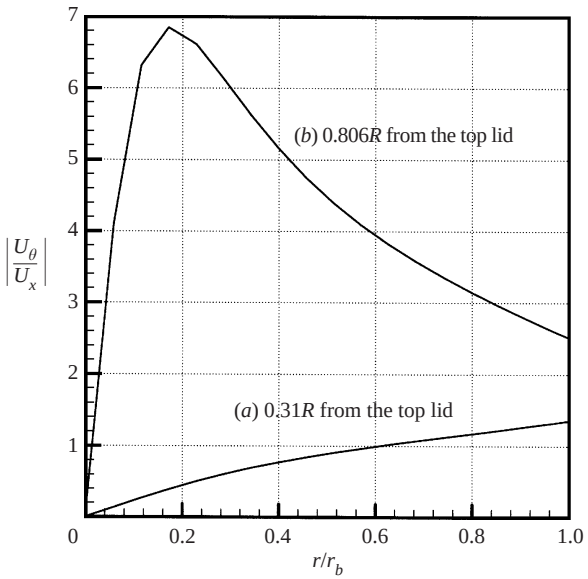

FIGURE 20. Calculated swirl ratio profiles at representative locations upstream of the (*a*) first, and (*b*) second vortex-breakdown bubbles for $Re = 1900$, $H/R = 2$. For reference, the upstream stagnation points for the first and second bubbles are located at $0.4R$ and $0.9R$, respectively, from the stationary cover. r_b is the maximum radius of the first bubble.

(see figure 3), introducing a controlled asymmetric disturbance in the apparatus causes the folds at the downstream end of the bubble – the intersection of the spiralling stable and unstable manifolds of the spiral-in saddle with the plane of section – to intensify. Clearly figure 19(*a–c*) illustrates the same trends. In fact the bubble shape shown in figure 19(*c*) is strikingly similar to that observed experimentally by Spohn *et al.* (1998) when visualization tracers were introduced from a solder wire on the stationary cover. Sotiropoulos & Ventikos (2001) argued that the small differences in the shape of the bubbles obtained with different visualization methods in Spohn *et al.* (1998) should be due to different disturbance levels introduced by the various techniques. Figure 19(*a–c*) along with our experimental images shown in figure 3 provide further support for this assertion. A possible explanation of the quasi-periodic dynamics of the second vortex-breakdown bubble also emerges from the results shown in figure 19(*d–f*) and the relative intensity of the swirling motion in the vicinity of the first and second vortex-breakdown bubbles. Figure 20 shows calculated profiles of the swirl ratio (ratio of the azimuthal, U_θ, to axial, U_x, velocity components) at axial locations upstream of the first and second bubbles, respectively, for the $Re = 1900$ and $H/R = 2$ case. As seen in this figure, the swirl ratio in the vicinity of the second bubble is approximately one order of magnitude greater. This trend is due to the fact that the axial velocity is reduced dramatically near the second bubble while the azimuthal velocity is nearly constant in the vicinity of the two bubbles. It can be readily seen from (7.1) that varying ω from 0.5 to 2.0 while keeping all other parameters constant would cause the maximum local swirl ratio upstream of the bubble in the model system to vary from approximately less than 1 (figure 19*c*) to greater than 4 (figure 19*f*), respectively. Based on these observations and the results shown in figure 20 we argue herein that the very high swirl level characterizing the second bubble stabilizes the Lagrangian orbits and leads to the axisymmetric images observed in the laboratory. It is remarkable

to note that the velocity field in the laboratory apparatus possesses the same level of three-dimensional disturbances for the first and second bubbles. Yet, it appears that the effect of these disturbances on the Lagrangian dynamics is almost entirely mitigated when vortex-breakdown bubbles occur at high swirl levels.

8. Summary and closing remarks

We report herein the first experimental evidence confirming and further clarifying previous theoretical and computational results concerning the rich Lagrangian dynamics in the interior of steady vortex-breakdown bubbles. We have developed the first non-intrusive visualization technique for constructing Poincaré maps in the laboratory and obtained experimental maps that are in good agreement with the numerical simulations. Finally, we argue that a simple Eulerian quantity, the swirl ratio, is the key parameter that determines the complexity of the Lagrangian dynamics. Vortex breakdown bubbles occurring at sufficiently high swirl intensities can exhibit integrable quasi-periodic dynamics, even though they form within a three-dimensional flow.

The present work, along with the previous experimental study of Spohn *et al.* (1998) and the numerical simulations of Sotiropoulos & Ventikos (2001) and Sotiropoulos *et al.* (2001), reinforces the similarities between vortex-breakdown bubbles in the confined geometry and those forming in open systems (Sarpkaya 1971*a*, *b*; Faler & Leibovich 1977). Our findings further point to the conclusion that a great deal of caution should be exercised when dye visualization experiments of vortex breakdown flows are interpreted to derive conclusions about the Eulerian aspects of the phenomenon. For example, the results we have presented herein suggest that Eulerian unsteadiness is not an intrinsic feature of the bubble-mode of vortex breakdown. Of course, under certain flow conditions vortex-breakdown bubbles in diffuser geometries (as well as in the container problem) also form within an unsteady, from the Eulerian standpoint, flow. Both Sarpkaya (1971*a*, *b*) and Faler & Leibovich (1977) have described bubbles whose upstream stagnation point tends to dart back and forth along the axis in a highly unsteady manner. Unsteady vortex-breakdown flow fields have also been documented in more recent numerical (Spall, Gatski & Ash 1990) and experimental (Brücker & Althaus 1992) studies. However, Sarpkaya (1971*a*, *b*) has also reported that under certain flow conditions vortex-breakdown bubbles whose location is very stable in time can be realized in the laboratory. Even for these cases, however, the flow in the interior of the bubble has been described as being quite unsteady, dominated, according to Sarpkaya (1971*a*, *b*), by the gyrations of a tilted toroidal ring. Furthermore, both Sarpkaya (1971*a*, *b*) and Faler & Leibovich (1977) have described essentially the same highly unsteady bursting mechanism via which the bubble exchanges fluid with the surrounding flow. Our present results show that this apparent unsteadiness of dye transport and the temporally complex emptying mechanism observed in the laboratory do not necessarily imply that the transporting velocity field is unsteady. Arbitrarily long Lagrangian transients in a steady three-dimensional flow field with rich dynamics could produce highly unsteady dye transport patterns and, thus, lead to the false conclusion of Eulerian unsteadiness.

An important structural characteristic of vortex-breakdown bubbles in diffuser geometries is the temporary appearance of a filament of dye on the axis inside the bubble (see figure 1*a*). Faler & Leibovich (1977) reported that this screw-worm-like filament appeared in a seemingly random manner along the axis even after the dye supply had been interrupted. The random temporal variations of dye concentration

within this filament are consistent with the random variations of light intensity in the vicinity of the axis in the images shown in figure 4. As we have already discussed, such variations are due to the chaotic stirring of tracers as they recirculate along Šil'nikov orbits of arbitrarily long period. Furthermore, tracers initially trapped in the interior of the bubble would have to arrive in this columnar region before they can exit the bubble along the unstable manifolds of the spiral-in saddle. Since such tracers have to cross the multiple fractal barriers (cantori) that foliate the internal toroidal region, they will not arrive in the vicinity of the axis in a continuous manner but rather in a sequence of random bursting events. The motion of such tracers would further contribute to the random variations of light intensity within the on-axis filament. Once again, such complex temporal variations in the transport of dye tracer do not necessarily imply that the transporting Eulerian flow is unsteady – Faler & Leibovich (1977), however, reported that the velocity fields in their experiment were indeed unsteady as the axial location of all vortex-breakdown bubbles they observed appeared to drift back and forth along the axis in a random manner.

The persistence of dye in the interior of vortex-breakdown bubbles has also been documented by both Sarpkaya (1971*a*, *b*) and Faler & Leibovich (1977) in their diffuser experiments. They both reported that the inner region of the bubble remained visible for as long as 20 s after the dye supply was interrupted. Obviously in our experiments the tracer residence times appear to be considerably longer, at least in terms of dimensional time. This trend, however, may be related to the fact that the container flow is steady from an Eulerian perspective, while Faler & Leibovich (1977) studied vortex breakdown in an unsteady Eulerian flow. The presence of even a very small unsteady component of the flow could obviously have a dramatic impact on the dynamics of the interior of the bubble and, thus, affect considerably the residence times of upstream-originating tracers.

A link between swirl intensity and the degree of axisymmetry of vortex-breakdown bubbles has been alluded to by Sarpkaya (1971*a*, *b*). In his pioneering 1971*a* paper he states: "... For larger swirl or vane angles, the breakdown form moved progressively upstream and at a definite combination of swirl and flow, the bubble became a smooth and nearly symmetric body ...". It is important to recognize, however, that neither Sarpkaya's work nor any other of the previously reported experimental and computational studies of vortex breakdown in open systems were carried out with the rich Lagrangian properties of the phenomenon in mind. Further experimental and computational studies are required before the significance of our findings can be fully understood in the context of vortex breakdown in open systems. We hope that our work on the confined flow and our discussion in this section will stimulate and help guide such studies. Additional work is also needed in order to develop a formal theory that explains and quantifies the apparent link between swirl intensity and the richness of the Lagrangian dynamics. Such a theory could lead to a rigorous framework for controlling mixing efficiency and the residence time distribution in vortex-breakdown bubbles in flows of technological significance.

Our work so far has focused on the dynamics of vortex-breakdown bubbles in the container flow. There is, however, experimental and computational evidence suggesting that the global recirculating flow within the container may also exhibit rich Lagrangian dynamics. Experiments (Spohn *et al.* 1998) and computations (Sotiropoulos & Ventikos 1998, 2001) have shown, for instance, that the flow within the sidewall boundary layers is dominated by spiral modes, which in the unsteady regime evolve into quasi-stationary spiral vortices. Furthermore, Goldshtik *et al.* (1992) and Husain *et al.* (1995) have documented a perplexing Lagrangian phenomenon in this flow,

which they dubbed 'anomalous separation'. They observed that an initially homogeneous particle–fluid mixture in a container similar to that we have studied herein separates into its components shortly after the lid begins to rotate. Kinematic effects are suspected as the separating mechanism (Goldshtik *et al.* 1992; Husain *et al.* 1995), but a satisfactory explanation of this intriguing phenomenon has yet to be developed. Combined computational and experimental studies of Lagrangian transport within the entire container using the techniques that we have developed for the vortex-breakdown bubbles will be needed in order to illuminate these phenomena.

We thank Yiannis Ventikos, Todd Taylor and Anny Huang for assisting with the apparatus design and preliminary experiments. The computations were performed on the multiprocessor Silicon Graphics Origin 2000 system of the Office of Information Technology at the Georgia Institute of Technology. F. S. and T. C. L. were supported by NSF grant CMS-9875691.

REFERENCES

Aref, H. 1984 Stirring by chaotic advection. *J. Fluid Mech.* **143**, 1–21.

Ashwin, P. & King, G. P. 1997 A study of particle paths in non-axisymmetric Taylor–Couette flows. *J. Fluid Mech.* **338**, 341–362.

Broer, H. W. & Vetger, G. 1984 Subordinate Šil'nikov bifurcations near some singularities of vector fields having low codimension. *Ergod. Theor. Dyn. Syst.* **4**, 509–525.

Brücker, C. & Althaus, W. 1992 Study of vortex breakdown by particle tracking velocimetry (PTV). Part 1: Bubble-type vortex breakdown. *Exps. Fluids* **13**, 339–349.

Delery, J. M. 1994 Aspects of vortex breakdown. *Prog. Aerospace Sci.* **30**, 1–59.

Escudier, M. P. 1984 Observations of the flow produced in a cylindrical container by a rotating endwall. *Exps. Fluids* **2**, 189–196.

Escudier, M. P. 1988 Vortex breakdown: Observations and explanations. *Prog. Aerospace Sci.* **25**, 189–229.

Faler, J. H. & Leibovich, S. 1977 Disrupted states of vortex flow and vortex breakdown. *Phys. Fluids* **20**, 1385–1400.

Fountain, G. O., Khakar, D. V., Mezić, I. & Ottino, J. M. 2000 Chaotic mixing in a bounded three-dimensional flow. *J. Fluid Mech.* **417**, 265–301.

Fountain, G. O., Khakar, D. V. & Ottino, J. M. 1998 Visualization of three-dimensional chaos. *Science* **281**, 683–686.

Gelfgat, A. Yu., Bar-Yoseph, P. Z. & Solan, A. 1996 Stability of confined flow with and without vortex breakdown. *J. Fluid Mech.* **311**, 1–36.

Goldshtik, M., Husain, H. S. & Hussain, F. 1992 Kinematic separation of mixtures. *Phys. Rev.* A **45**, 8611–8616.

Holmes, P. 1984 Some remarks on chaotic particle paths in time-periodic, three-dimensional swirling flows. *Contemp. Maths* **28**, 393–404.

Hourigan, K., Graham, L. J. W. & Thompson, M. C. 1995 Spiral streaklines in pre-vortex breakdown regions of axisymmetric swirling flows. *Phys. Fluids* **7**, 3126.

Husain, H. S., Hussain, F. & Goldshtik, M. 1995 Anomalous separation of homogeneous particle-fluid mixtures: Further observations. *Phys. Rev.* E **52**, 4909–4923.

Leibovich, S. 1978 The structure of vortex breakdown. *Annu. Rev. Fluid Mech.* **10**, 221–246.

Leibovich, S. 1984 Vortex stability and breakdown: Survey and extension. *AIAA J.* **22**, 1192–1206.

Lopez, J. M. 1990 Axisymmetric vortex breakdown. Part 1. Confined swirling flow. *J. Fluid Mech.* **221**, 533–552.

Lopez, J. M. & Perry, A. D. 1992 Axisymmetric vortex breakdown. Part 3. Onset of periodic flow and chaotic advection. *J. Fluid Mech.* **234**, 449–471.

Kroujiline, D. & Stone, H. A. 1999 Chaotic streamlines in steady bounded three-dimensional Stokes flows. *Physica* D **130**, 105–132.

MacKay, R. S. 1994 Transport in 3D volume-preserving flows. *J. Nonlinear Sci.* **4**, 329–354.

MacKay, R. S., Meiss, J. D. & Percival, I. C. 1984 Transport in Hamiltonian systems. *Physica* D **13**, 55–81.

Malhotra, N., Mezić, I. & Wiggins, S. 1999 Patchiness: A new diagnostic for Lagrangian trajectory analysis in time-dependent fluid flows. *Intl J. Bifurcation Chaos* **8**, 1053.

Mezić, I. & Sotiropoulos, F. 2002 Ergodic theory and experimental visualization of invariant sets in chaotically advected flows. *Phys. Fluids* **14**, 2235–2243.

Mezić, I. & Wiggins, S. 1994 On the integrability and perturbation of three-dimensional fluid flows with symmetry. *J. Nonlinear Sci.* **4**, 157–194.

Mezić, I. & Wiggins, S. 1999 A method for visualization of invariant sets of dynamical systems based on the ergodic partition. *Chaos* **9**, 213.

Peckham, D. H. & Atkinson, S. A. 1957 Preliminary results of low speed wind tunnel tests on a gothic wing of aspect ratio 1.0. *ARC Tech. Rep. CP* 508*, TN Aero*. 2504.

Sarpkaya, T. 1971*a* On stationary and travelling vortex breakdowns. *J. Fluid Mech.* **45**, 545–559.

Sarpkaya, T. 1971*b* Vortex breakdown in swirling conical flows. *AIAA J.* **9**, 1792–1799.

Sarpkaya, T. 1995 Vortex breakdown and turbulence. *AIAA Paper* 95-0433.

Šil'nikov, L. P. 1965 A case of the existence of a denumerable set of periodic motions. *Sov. Math. Dokl.* **6**, 163–166.

Sotiropoulos, F. & Ventikos, Y. 1998 Transition from bubble-type vortex breakdown to columnar vortex in a confined swirling flow. *Intl J. Heat Fluid Flow* **19**, 446–458.

Sotiropoulos, F. & Ventikos, Y. 2001 The three-dimensional structure of confined swirling flows with vortex breakdown. *J. Fluid Mech.* **426**, 155–175.

Sotiropoulos, F., Ventikos, Y. & Lackey, T. C. 2001 Chaotic advection in three-dimensional stationary vortex-breakdown bubbles: Šil'nikov's chaos and the Devil's Staircase. *J. Fluid Mech.* **444**, 257–297.

Spall, R. E., Gatski, T. B. & Ash, R. L. 1990 The structure and dynamics of bubble-type vortex breakdown. *Proc. R. Soc. Lond.* A **429**, 613.

Spohn, A., Mory, M. & Hopfinger, E. J. 1993 Observations of vortex breakdown in an open cylindrical container with rotating bottom. *Exps. Fluids* **13**, 70–77.

Spohn, A., Mory, M. & Hopfinger, E. J. 1998 Experiments on vortex breakdown in a confined flow generated by a rotating disk. *J. Fluid Mech.* **370**, 73–99.

Stevens, J. L., Celik, Z. Z., Cantwell, B. J. & Lopez, J. M. 1996 Experimental study of vortex breakdown in a cylindrical swirling flow. *Joint Inst. for Aeronautics and Acoustics Rep. JIAA TR* 117. Dept. of Aeronautics and Astronautics, Stanford University.

Stevens, J. L., Lopez, J. M. & Cantwell, B. J. 1999 Oscillatory flow states in an enclosed cylinder with a rotating endwall. *J. Fluid Mech.* **389**, 101–118.

Stone, H. A., Nadim, A. & Strogatz, S. H. 1991 Chaotic streamlines inside drops immersed in steady Stokes flows. *J. Fluid Mech.* **232**, 629–646.

Wiggins, S. 1990 *Introduction to Applied Nonlinear Dynamical Systems and Chaos*. Springer.